David Taylor Research Center

Bethesda, MD 20084-5000

DTRC/SHD-1355-02 December 1991

Ship Hydromechanics Department

Departmental Report

THE EFFECT OF TURBULENCE INGESTION ON PROPELLER BROADBAND THRUST

by

C.W. Jiang, M.S. Chang and Y.N. Liu

DTRC/SHD 1355-02 The Effect of Turbulence Ingestion on Propeller Broadband Thrust

UNCLASSIFIED
SECURITY CLASSIFICATION OF THIS PAGE

REPORT DOCUMENTATION PAGE

1a. REPORT SECURITY CLASSIFICATION UNCLASSIFIED	1b. RESTRICTIVE MARKINGS
2a. SECURITY CLASSIFICATION AUTHORITY	3. DISTRIBUTION / AVAILABILITY OF REPORT Approved for public release; Distribution is unlimited
2b. DECLASSIFICATION / DOWNGRADING SCHEDULE	
4. PERFORMING ORGANIZATION REPORT NUMBER(S) DTRC/SHD-1355-02	5. MONITORING ORGANIZATION REPORT NUMBER(S)
6a. NAME OF PERFORMING ORGANIZATION David Taylor Research Center 6b. OFFICE SYMBOL (If applicable) Code 1542	7a. NAME OF MONITORING ORGANIZATION
6c. ADDRESS (City, State, and Zip Code) Bethesda, MD 20084-5000	7b. ADDRESS (City, State, and Zip Code)
8a. NAME OF FUNDING / SPONSORING ORGANIZATION ONR 8b. OFFICE SYMBOL (If applicable)	9. PROCUREMENT INSTRUMENT IDENTIFICATION NUMBER
8c. ADDRESS (City, State, and Zip Code) ONR Arlington, VA 22217-5000	10. SOURCE OF FUNDING NUMBERS PROGRAM ELEMENT NO. / PROJECT NO. / TASK NO. R0092 / WORK UNIT ACCESSION NO. 0101224N
11. TITLE (Include Security Classification) THE EFFECT OF TURBULENCE INGESTION ON PROPELLER BROADBAND THRUST	
12. PERSONAL AUTHOR(S) C. W. Jiang, M. S. Chang, and Y. N. Liu	
13a. TYPE OF REPORT Final	13b. TIME COVERED FROM_____ TO_____
14. DATE OF REPORT (Year, Month, Day) 1991, December	15. PAGE COUNT 45
16. SUPPLEMENTARY NOTATION	

17. COSATI CODES			18. SUBJECT TERMS (Continue on reverse if necessary and identify by block number)
FIELD	GROUP	SUB-GROUP	propeller thrust spectrum ingest turbulence propeller

19. ABSTRACT (Continue on reverse if necessary and identify by block number)

This report presents the theoretical prediction of the low frequency unsteady broadband thrust for propellers/rotors in a turbulent flow, such as those on any surface ship. Broadband thrust forces are predicted by the use of a new correlation method and are compared with existing theoretical models based on both correlation and spectrum approaches. In contrast to the available theories, the new theory predicts low blade rate humps and broadband forces simultaneously. For a homogeneous and isotropic turbulent inflow and for a given advance coefficient, turbulence length scale and turbulence level, the present theory produces an unsteady broadband thrust level which is proportional in the high frequency region to the third power of ship speed. At low frequencies, predictions of propeller unsteady thrust spectra show peaks near the first and second blade rate frequencies and those peaks skew to the higher frequency side of the blade rate frequencies. The physics of the phenomena are discussed and numerical results are compared with limited experimental data.

20. DISTRIBUTION / AVAILABILITY OF ABSTRACT ☒ UNCLASSIFIED/UNLIMITED ☐ SAME AS RPT ☐ DTIC USERS	21. ABSTRACT SECURITY CLASSIFICATION UNCLASSIFIED
22a. NAME OF RESPONSIBLE INDIVIDUAL Chen-Wen Jiang	22b. TELEPHONE (Include Area Code) (301) 227-1324 22c. OFFICE SYMBOL Code 1542

DD FORM 1473, 84 MAR

83 APR edition may be used until exhausted
All other editions are obsolete

SECURITY CLASSIFICATION OF THIS PAGE
UNCLASSIFIED

CONTENTS

Figures

Nomenclature

A_s	Filter function
b	Blade spacing
C	Blade section chord length
D	Propeller diameter
f(r)	Longitudinal velocity correlation function
f_M	Meanline shape function
g(r)	Transverse velocity correlation function
$G_{ij}(\omega)$	Velocity correlation in frequency domain
$H(\omega)$	Aerodynamic response function
i_T	Total rake
$J = V_s/nD$	Advance coefficient
$K(\omega)$	Sears function
k	Wave number
$\ell(t)$	Hydrodynamic force
n	Propeller rotational speed, rps
P	Pitch of blade section
r	Radial coordinate or distance between two points
R	Propeller radius
$R_{ij}(\tau)$	Velocity correlation in time domain
u	Root mean square of turbulence
u_i	Turbulent velocity in i-th direction
U(r)	Resultant velocity at propeller radius r
V_a	Axial velocity at propeller plane for a given radial location
V_s	Ship speed
#	Lbs
ω	Frequency
Ω	Shaft rate frequency
Ω'	Blade rate frequency
q_s	Skew angle
Λ	Turbulence integral length scale

ρ	Fluid density
ϕ	Propeller blade pitch angle
ϕ_i	One dimensional turbulence spectrum
Φ	Wave number spectrum of turbulence
Ψ	Broadband unsteady thrust spectrum
Ψ^*	Broadband unsteady thrust/ω^3

Abstract

This report presents the theoretical prediction of the low frequency unsteady broadband thrust for propellers/rotors in a turbulent flow, such as those on any surface ship. Broadband thrust forces are predicted by the use of a new correlation method and are compared with existing theoretical models based on both correlation and spectrum approaches. In contrast to the available theories, the new theory predicts low blade rate humps and broadband forces simultaneously. For a homogeneous and isotropic turbulent inflow and for a given advance coefficient, turbulence length scale and turbulence level, the present theory produces an unsteady broadband thrust level which is proportional in the high frequency region to the third power of ship speed. At low frequencies, predictions of propeller unsteady thrust spectra show peaks near the first and second blade rate frequencies and those peaks skew to the higher frequency side of the blade rate frequencies. The physics of the phenomena are discussed and numerical results are compared with limited experimental data.

Administrative Information

This work was performed at the David Taylor Research Center (DTRC) in Bethesda, Maryland 20084-5000 with work unit 1-1904-301, with funding from the Office of Naval Research, element 0101224N.

Introduction

The unsteady forces generated by a propeller/rotor consist of periodic force components and a broadband force component. The narrowband periodic force components occur at multiples of the blade passage frequency and are considered to result from the unsteady pressure distribution on the propeller blades. These unsteady pressures are caused by the non-uniform inflow or by cavitation, such as for the propellers on surface ships. Force

spectra from this non-uniform inflow are narrowband at the blade rates. The high frequency broadband noise is due to vortex shedding by the propeller blades. Although designers are careful to reduce these unsteady force sources, laboratory experiments indicate that an unexpected broadband force occurs at first and second blade rate frequencies. This low frequency broadband force is due to the interaction of the inflow turbulence with the propeller blades. The inflow turbulence ingested on the propeller blades is generated in the hull boundary layer and in the boundary layers on all the appendages upstream of the propeller, superposed on the ambient free-stream turbulence. Therefore, the inflow turbulence may contain a broad range of length scales. This report addresses the effects of turbulence on broadband forces generated by propeller blades regardless of the source of the turbulence.

The unsteady force caused by turbulence ingestion has been studied by several investigators in the past. Most previous studies are based upon special assumptions and, thus, lack generality. Sevik [1] considered the forward speed to be much greater than the propeller rotational speed and, therefore, regarded the blades as rotationally stationary with respect to the turbulence. This assumption implied that the blades are rotationally uncorrelated. He measured the unsteady thrust on a ten-bladed rotor operating in a water tunnel downstream of screen-generated turbulence. The experimental measurements show humps near blade rate frequencies and its multiples which were not predicted from Sevik's theory. Thompson [2] extended this theory and performed additional experiments for rotors with different numbers of blades. The experimental results show that the magnitude of the broadband humps increases when the blade-to-blade spacing decreases. He included in his analysis the blade to blade circumferential correlations in a zero forward speed sense. In comparison to the experiments, his theoretical results produced consistently higher humps. Chandrashekhara [3] examined only the cases for which the circumferential correlation length was larger than a blade spacing. Mani [4], Homicz and George [5], Amiet [6], and Blake [7] considered the ro-

tor forces and noises radiated by turbulence with a given wave spectrum. Mani [4] showed that the radiated sound spectrum from a rotor operating in a turbulent inflow has humps centered at the blade rate frequencies and its multiples. The width of those humps was found in his experiments to be related to the ratio of the turbulence length scale to the blade spacing. Blake [7] considered the case of a rotor with a small advance coefficient and a turbulence length scale considerably smaller than the length of the blade span. Simple results are obtained from asymptotic expansion of small and large correlation lengths. The small correlation result approaches the result of Sevik's analysis, and the large correlation theory predicts the narrow bandwidth humps at blade rate frequencies. Although Blake's model predicts the humps at the blade rate frequency, the hump amplitudes above the smooth broadband force spectrum curve do not exhibit the decay phenomena observed in experiments. Recently, Martinez [8] extended Sevik's theory by including the propeller rotational speed in the correlation area, a term defined in [1]. His results show only small humps at blade rates and were again unable to explain the near blade-rate humps demonstrated in experiments.

In the present report, the correlation analysis follows Sevik's approach [1], but removes the simplification of the velocity correlation tensor used in [1] and [8]. The blade rotational effect is correctly preserved in the analysis and the results resemble the experimental observation. Numerically, for a given turbulence correlation function, the statistical properties of the unsteady angle of attack encountered by the moving blade are evaluated at each time step. Then the force spectrum is obtained from a Fourier transformation of the computed time history of those unsteady angles of attack. The next two sections outline the fundamental approaches and the corresponding computational procedures. Numerical examples are included for the thrust spectrum of isotropic turbulence on a rotor using both correlation and spectrum approaches. These results are compared with existing experiments. A flow chart of the present numerical turbulence ingestion (TI) model is given in Figure 1; the blade surface is

divided into chordwise strips along the span. Each strip is considered as a two-dimensional (2-D) section with unsteady lift concentrated at the quarter-chord of that section. As is indicated in Figure 1, the two critical components of the model are the inflow turbulence characteristics and the transfer function between the turbulence intensity spectrum and the unsteady forces. In the given examples, the Sears function is used as the fluid dynamic transfer function.

Theoretical Approach

The analysis of turbulence-generated propeller broadband force can be approached with two different techniques. One is the spectrum approach and the other is the correlation approach. These two approaches should lead to the same results if the specified spectrum form and correlation function describe the same turbulence characteristics. The authors prefer the correlation method because it is the more direct approach and is easier to apply numerically. However, for completeness of the study, the spectrum approach is included in this report. Results from both approaches will be compared in the discussions.

Spectrum Approach

This section follows the procedure described in Blake [7], which assumes that the turbulence is convected frozen (Taylor's hypothesis) and the turbulent characteristics are represented as a product of functions in each direction (separation of variables). With the turbulent inflow component normal to the blade, u_2 in Figure 2, expressed in terms of its Fourier transform:

$$u_2(\vec{k},\omega) = \frac{1}{(2\pi)^3}\int\int\int\int u_2(\vec{x},t)e^{-i(\vec{k}\cdot\vec{x}-\omega t)}d\vec{x}dt \qquad (1)$$

where $\vec{}$ denotes the vector in terms of the coordinates in the propeller plane (x_1, x_3) and its normal (x_2), the lift per unit radius on the s-th blade written in terms of the Fourier components of the incident upwash, $u_2(\vec{k},\omega)$, is

$$dL_s(\omega)/dr = \rho\pi C u_2(\vec{k},\omega)U(r)L_{2D}(k_1C/2)e^{i(k_3r+k_{12}sb-\omega t)} \tag{2}$$

where L_{2D} is the two-dimensional lift due to a unit disturbance, C is the blade chord length, b is the blade spacing at the radius r, k_{12} equals $k_1\cos\phi + k_2\sin\phi$, ϕ is the blade pitch angle, and U(r) is the resultant velocity into the blade at radius r. The net force on an N-bladed propeller in the i-th direction due to the $(\vec{k},\omega)$ turbulence contribution is found by summing over all the blades and integrating over the radius from the propeller hub (R_H) to tip (R_T)

$$F_i(\vec{k},\omega) = \int_{R_H}^{R_T} \rho\pi C u_2(\vec{k},\omega)U(r)n_i(\phi)L_{2D}(k_1C/2)\sum_{s=0}^{N-1} e^{i(k_3r+k_{12}sb-\omega t)}dr \tag{3}$$

where $n_i(\phi)$ is the direction cosine in the i-th direction of the blade. The summation over the N blades in equation (3) is called a filtering function, denoted A_s, and is

$$\begin{aligned} A_s(k_{12}b) &\equiv \sum_{s=0}^{N-1} e^{ik_{12}sb} \\ &= \frac{\sin(Nk_{12}b/2)e^{[i(N-1)k_{12}b/2]}}{\sin(k_{12}b/2)} \end{aligned} \tag{4}$$

Substituting this expression back into equation (3), the net force becomes

$$F_i(\vec{k},\omega) = \int_{R_H}^{R} \rho\pi C u_2(\vec{k},\omega)U(r)n_i(\phi)L_{2D}(k_1C/2)A_s(k_{12}b)e^{-i(k_3r-\omega t)}dr \tag{5}$$

and the frequency spectrum of the fluctuating force, $\Psi_{ii}(\omega)$, becomes

$$\Psi_{ii}(\omega) = \int_{k_1}\int_{k_2}\int_{k_3}\int_{R_H}^{R}\int_{R_H}^{R} \rho^2\pi^2 C^2 \mid L_{2D}(k_1 C/2) \mid^2 \mid A_s(k_{12}b) \mid^2$$

$$U(r_1)U(r_2)\Phi_{22}(\vec{k},\omega)n_i(\gamma_1)n_i(\gamma_2)e^{ik_3(r_2-r_1)}dr_2 dr_1 d\vec{k} \qquad (6)$$

where $\Phi_{22}(\vec{k},\omega)$ is the wave number spectrum of the turbulent field. Equation (6) is the fundamental form of the spectrum approach. It is clearly seen that the major task of the analysis is in the specification of the wave number spectrum of the turbulent field $\Phi_{22}(\vec{k},\omega)$ and the evaluation of the multiple integrals. In general, the spectrum form $\Phi_{22}(\vec{k},\omega)$ associated with a moving body is not known, and the prediction of $\Psi_{ii}(\omega)$ with triple integration over $\vec{k}$ is impractiable. Nevertheless, the analytical results associated with some simple forms of $\Phi_{22}(\vec{k},\omega)$ could provide a good approximation to reality and lead to a better understanding of the overall features of $\Psi_{ii}(\omega)$.

By applying Taylor's hypothesis that the turbulence convects over the blade with the resultant velocity and without decay, and by assuming that the wave number spectrum can be separated into directions along the resultant velocity (k_1), the radial direction (k_3), and the normal direction (k_2), the turbulence spectrum becomes

$$\Phi_{22}(\vec{k},\omega) = \bar{u_2^2}\phi_1(k_1)\phi_2(k_2)\phi_3(k_3)\delta[\omega - U(r)k_1] \qquad (7)$$

Furthermore, we assume that $\phi_i(k_i)$ takes a form of

$$\phi_i(k_i) = \frac{1}{\pi}\frac{\Lambda_i}{1+(\Lambda_i k_i)^2} \qquad (8)$$

where $2\Lambda_i$ represents the integral length scale of u_2 in the i-th wave vector direction. When the radial integral length scale is small with respect to the blade span, i.e.,$\phi_3(k_3) \simeq \Lambda_3/\pi$ and the radial direction wave number is small, i.e., $k_3 R \ll 1$, the force spectrum , equation (6) becomes

$$\begin{aligned}
\Psi_{ii}(\omega) &= \int_{k_1}\int_{k_2}\int_{R_H}^{R_T} \rho^2\pi C^2\Lambda_3 \mid L_{2D}(k_1C/2) \mid^2 \mid A_s(k_{12}b) \mid^2 \\
&\quad U^2(r)\bar{u_2^2}\phi_1(k_1)\phi_2(k_2)n_i^2(\phi)\delta[\omega - U(r)k_1]drdk_1dk_2 \\
&= \int_{k2}\int_{R_H}^{R_T} \rho^2\pi C^2\Lambda_3 \mid L_{2D}(\frac{\omega C}{2U}) \mid^2 \mid A_s[(k_2\sin\phi + \frac{\omega}{U}\cos\phi)b] \mid^2 \\
&\quad U^2(r)\bar{u_2^2}\phi_1(\omega/U)\phi_2(k_2)n_i^2(\phi)drdk_2 \qquad (9)
\end{aligned}$$

For simplification, the average spanwise lift amplitude as a function of wave number has been used in the last formulation. Then the turbulence spectrum can be moved outside of the radial integral. The discrete, numerical expression of equation (9) becomes

$$\begin{aligned}
\Psi_{ii}(\omega) &= \sum_{\delta k_2}\phi_2(k_2)\sum_{\delta R}\rho^2\pi C^2\Lambda_3 \mid L_{2D}(\frac{\omega C}{2U}) \mid^2 \mid A_s[(k_2\sin\phi + \frac{\omega}{U}\cos\phi)b] \mid^2 \\
&\quad U^2\bar{u_2^2}\phi_1(\omega/U)n_i^2(\phi) \qquad (10)
\end{aligned}$$

Equation (10) entails summation over the blade elements and the wave number and it is numerically more managable than equation (6). The application of this model will be presented in a later section and the results will be discussed. For the case of small advanced coefficient and small hub, $R_T \gg R_H$, equation (9) can be further reduced to

$$\Phi_{ii}(\omega) = \frac{\pi^2}{3}[\rho(\Omega R_T)^2]^2(CR_T)^2\bar{u_2^2}/(\Omega R_T)^2 \mid L_{2D}(\frac{\omega C}{U_T}) \mid^2 (2\Lambda_3/R_T)$$
$$n_i^2(\gamma)\frac{1}{U_T}\phi_1(\frac{\omega}{U_T})\int_{-\infty}^{\infty} \mid A_s[(k_2 \sin\gamma + \frac{\omega}{U_T}\cos\gamma)b] \mid^2$$
$$\phi_2(k_2)dk_2 \qquad (11)$$

where U_T is the resultant tip speed $\sqrt{V^2 + (R_T\Omega)^2}$ (V is axial inflow velocity). Blake[7] obtained the asymptotic solutions of the above equation. Evaluation of the integral is determined by the relative width of the turbulence spectrum, $\phi_2(k_2)$, and the filter function, $\mid A_s[(k_2 \sin\gamma + \frac{\omega}{U_T}\cos\gamma)b] \mid^2$. When the band of $\phi_2(k_2)$ is greater than the range of the filter function, i.e., the axial integral length parameter, $2\Lambda_2$, is smaller than the blade spacing projected in the axial direction (small correlation length), the last equation can be simplified to

$$\Phi_{ii}(\omega) = \frac{8\pi^2}{3n_s}(\frac{1}{2}\rho V^2)^2 {R_T}^4(\frac{C}{R_T})^2(\frac{\pi}{J})^2\frac{\bar{u_2^2}}{V^2}\frac{2\Lambda_3}{R_T}\frac{\Lambda_1/\pi R_T}{1+(\Lambda_1\omega/\Omega_s R_T)^2}$$
$$\frac{1}{1+\pi\omega C/\Omega_s R_T} \qquad (12)$$

On the other hand, when the axial integral length parameter, $2\Lambda_2$, is greater than the blade spacing projected in the axial direction (large correlation length), equation (11) becomes

$$\Phi_{ii}(\omega) = \frac{8N\pi^2}{3n_s}(\frac{1}{2}\rho V^2)^2 {R_T}^4(\frac{C}{R_T})^2(\frac{\pi}{J})^2\frac{\bar{u_2^2}}{V^2}\frac{2\Lambda_3}{R_T}\frac{\Lambda_1/\pi R_T}{1+(\Lambda_1 mN/R_T)^2}$$
$$\frac{\mid A_s[(k_2 \sin\gamma + \frac{\omega}{U_T}\cos\gamma)b] \mid^2}{1+\pi mNC/R_T} \qquad (13)$$

where m is the number of the blade rate frequency; otherwise, $\Phi_{ii}(\omega)$ equals zero.

In examining equations (12) and (13), it is seen that equation (12) is a monotonically decreasing function of ω and it resembles the rotational uncorrelated results of Sevik [1]. Equation (13) contains only the blade rate humps with non-decayed amplitude above the rotational uncorrelated results. Neither of these approximations can be applied to predict the complete measured phenomena. In order to obtain a meaningful prediction, one has to go back to at least equation (11). Numerical results show that even (11) does not give satisfying predictions; only the results of equation (10) are in reasonable agreement with the measurements. Further discuissions of the spectrum approach will be given in the results section.

Correlation Approach

The derivations of the frequency spectrum of propeller thrust using the correlation approach are briefly discussed here. These derivations follow the theory of Sevik [1] except that the velocity correlation has been modified to incorporate propeller rotational effects. In order to calculate the characteristics of the fluctuating force over the blade surfaces, the blade is divided into a number of surface elements. The time-dependent forces acting on the various surface elements are related by virtue of spatial and temporal correlation of the velocity fluctuations in the approach stream as well as by virtue of the induced effects that take place between adjacent elements. In the following tensor equations, subscripts are used to denote the direction along the coordinate axes, while superscripts are used to denote the blade element involved. For example, $F_{ij}^{\alpha\beta}(t,\tau)$ denotes the hydrodynamic force acting on the α-th element in the direction i at the instant of time t caused by a velocity fluctuation of unit magnitude in the direction j on the β-th element at the instant τ. With this convention, the

hydrodynamic force acting on the α-th element at time t in the direction i, $\ell_i^\alpha(t)$, due to the influence of velocity fluctuation at all elements, β, and in all the directions, j, over all the time, τ, is expressed as

$$\ell_i^\alpha(t) = \int_{-\infty}^{t} F_{ij}^{\alpha\beta}(t,\tau) u_j^\beta(\tau) d\tau \tag{14}$$

where

$$\begin{aligned} i,j &= 1,2,3 \\ \alpha,\beta &= 1,2,...n \end{aligned}$$

Since $\ell_i^\alpha(t)$ is a random function of time in a turbulent flow, a statistical approach must be employed. If the inflow turbulence is time-invariant, the correlation function of unsteady forces, $\Phi_{ij}^{\alpha\beta}$, becomes

$$\begin{aligned} \Phi_{ij}^{\alpha\beta}(\tau) &\equiv E[\ell_i^\alpha(t)\ell_j^\beta(t+\tau)] \\ &= \lim_{T\to\infty} \frac{1}{T} \int_0^T \int_0^\infty \int_0^\infty F_{ik}^{\alpha\gamma}(\tau_1) F_{jm}^{\beta\delta}(\tau_2) u_k^\gamma(t-\tau_1) \\ &\quad u_m^\delta(t+\tau-\tau_2) d\tau_1 d\tau_2 dt \\ &= \int_0^\infty \int_0^\infty F_{ik}^{\alpha\gamma}(\tau_1) F_{jm}^{\beta\delta}(\tau_2) R_{km}^{\gamma\delta}(\tau+\tau_1-\tau_2) d\tau_1 d\tau_2 \end{aligned} \tag{15}$$

where

$$R_{km}^{\gamma\delta}(\tau+\tau_1-\tau_2) \equiv \lim_{T\to\infty} \frac{1}{T} \int_0^\infty u_k^\gamma(t-\tau_1) u_m^\delta(t+\tau-\tau_2) dt$$

The corresponding frequency spectrum of the correlated force fluctuations on the α-th element in the direction i due to the β-th element in the direction j can be found by taking the Fourier transform of the above

correlation tensor:

$$\Psi^{\alpha\beta}_{\ell_i\ell_j}(\omega) = \frac{1}{2\pi}\int_{-\infty}^{\infty}\Phi^{\alpha\beta}_{ij}(\tau)e^{-i\omega\tau}d\tau$$

$$= \frac{1}{2\pi}\int_{-\infty}^{\infty}\int_{0}^{\infty}\int_{0}^{\infty}F^{\alpha\gamma}_{ik}(\tau_1)d\tau_1 F^{\beta\delta}_{jm}(\tau_2)d\tau_2 R^{\gamma\delta}_{km}(\tau+\tau_1-\tau_2)d\tau$$

$$= [H^{\alpha\gamma}_{ik}(\omega)]^*[H^{\beta\delta}_{jm}(\omega)]G^{\gamma\delta}_{km}(\omega) \qquad (16)$$

where

$$H^{\alpha\gamma}_{ik}(\omega) \equiv \int_{0}^{\infty}F^{\alpha\gamma}_{ik}(\tau)e^{-i\omega\tau}d\tau$$

and

$$G^{\gamma\delta}_{km}(\omega) \equiv \frac{1}{2\pi}\int_{-\infty}^{\infty}R^{\gamma\delta}_{km}(\tau)e^{-i\omega\tau}d\tau$$

$H^{\alpha\beta}_{ik}(\omega)$ is the hydrodynamic frequency response function and $G^{\gamma\delta}_{km}(\omega)$ is the Fourier transform of the velocity correlation function. Equation (16) is the formula for predictions of unsteady forces due to inflow turbulence. When we apply this equation to the rotors, we have to specify $H^{\alpha\beta}_{ik}(\omega)$ and $G^{\gamma\delta}_{km}(\omega)$ according to the enviroments in which the rotors are operating. A computer code has been written to compute the $G(\omega)$ and $\Psi(\omega)$ for specified turbulence characteristics. To demonstrate the computation procedure, the analysis of an isotropic turbulence is given below for general discussion.

Isotropic Turbulence

In the present method, we shall first derive the velocity correlation function between points α and β. A detailed derivation for isotropic turbulence is given by Hinze [9] and is briefly described below. Longitudinal

correlation refers to the coordinate system in Figure 3. The origin of the coordinate system is at α and r is the distance between points α and β with components ξ_i along the axis x_i. In the plane of the $\alpha\beta$-line and the x_1-axis, the velocities at α and β can be resolved into the components u_{1*}, directed between these two points, and the components u_{2*}, which are perpendicular to the line-$\alpha\beta$. The velocity components along the x_1-axis at these two points are:

$$\begin{aligned} u_1^\alpha &= u_{1*}^\alpha \cos\varphi_1 - u_{2*}^\alpha \sin\varphi_1 \\ &= u_{1*}^\alpha \frac{\xi_1}{r} - u_{2*}^\alpha \sqrt{1 - \frac{\xi_1^2}{r^2}} \\ u_1^\beta &= u_{1*}^\beta \frac{\xi_1}{r} - u_{2*}^\beta \sqrt{1 - \frac{\xi_1^2}{r^2}} \end{aligned} \tag{17}$$

Let us define

$$\begin{aligned} \overline{u_{1*}^\alpha u_{1*}^\beta} &\equiv u^2 f(r) \\ \overline{u_{2*}^\alpha u_{2*}^\beta} &\equiv u^2 g(r) \end{aligned}$$

where u is the root-mean-square of turbulence and r is the distance along these two points. Because of invariance conditions, we have

$$\overline{u_{1*}^\alpha u_{2*}^\beta} = \overline{u_{2*}^\alpha u_{1*}^\beta} = 0$$

When we multiply u_1^α by u_1^β and take the mean value of the product, we get

$$R_{11} \equiv \overline{u_1^\alpha u_1^\beta}$$

$$= u^2[\frac{f(r)-g(r)}{r^2}\xi_1\xi_2 + g(r)] \tag{18}$$

Next, let us consider $\overline{u_1^\alpha u_2^\beta}$. From Figure 4, we have

$$u_1^\alpha = u_{1*}^\alpha \frac{\xi_1}{r} - u_{2*}^\alpha \sqrt{1-\frac{\xi_1^2}{r^2}}$$

$$u_2^\beta = u_{1*}^\beta \cos\varphi_2 + u_{2*}^\beta \frac{\cos\varphi_2}{\tan\varphi_1} + F(u_{3*}^\beta)$$

$$= u_{1*}^\beta \frac{\xi_2}{r} + u_{2*}^\beta \frac{\xi_1\xi_2}{r^2\sqrt{1-\frac{\xi_1^2}{r^2}}} + F(u_{3*}^\beta) \tag{19}$$

where $F(u_{3*}^\beta)$ is the term associated with the velocity component u_{3*}^β. This term is not given in detail because the invariance and isotropy conditions provide the zero mean for all terms containing the u_{3*}^β component. The invariance and isotropy conditions yield

$$\begin{aligned}\overline{u_{1*}^\alpha u_{2*}^\beta} &= \overline{u_{1*}^\alpha u_{3*}^\beta} \\ &= \overline{u_{2*}^\alpha u_{1*}^\beta} \\ &= \overline{u_{2*}^\alpha u_{3*}^\beta} \\ &= 0\end{aligned}$$

The correlation of u_1^α and u_2^β is determined as

$$R_{12} = \overline{u_1^\alpha u_2^\beta}$$

$$= u^2 \frac{f(r) - g(r)}{r^2} \xi_1 \xi_2 \tag{20}$$

In general, combining equations (18) and (20), we can write the velocity correlation as

$$R_{ij} = u^2 [\frac{f(r) - g(r)}{r^2} \xi_i \xi_j + g(r) \delta_{ij}] \tag{21}$$

where δ_{ij} is the Kronecker delta. The relationship between $f(r)$ and $g(r)$ can be derived from the continuity condition of fluid incompressibility.

$$\frac{\partial R_{ij}}{\partial \xi_j} = 0 \tag{22}$$

Substituting R_{ij} of equation (21) into equation (22) yields

$$f(r) + \frac{r}{2} \frac{\partial f(r)}{\partial r} = g(r) \tag{23}$$

From this relation between $f(r)$ and $g(r)$, the velocity correlation function can be expressed in terms of one scalar function, either f(r) or g(r), which gives

$$R_{ij} = u^2 [-\frac{1}{2r} \frac{\partial f(r)}{\partial r} \xi_i \xi_j + (f(r) + \frac{r}{2} \frac{\partial f(r)}{\partial r}) \delta_{ij}] \tag{24}$$

The longitudinal correlation function, $f(r)$, can be approximated by an exponential function

$$f(r) = e^{-r/\Lambda} \tag{25}$$

where Λ is the integral scale of the turbulence. This is equivalent to assuming that the turbulence spectrum is in the form as it is used in the spectrum approach. As has been verified by screen-generated turbulence, this is a good approximation for homogeneous and isotropic flow field.

For blades rotating in a turbulent field with rotational speed Ω, $r(\tau)$ is

$$r(\tau) \equiv \sqrt{(V\tau)^2 + r_\alpha^2 + r_\beta^2 - 2r_\alpha r_\beta \cos(\theta_\alpha - \theta_\beta + \Omega\tau)} \tag{26}$$

Equation (24) can be rewritten as:

$$R_{ij} = u^2[\frac{1}{2r\Lambda} r_i r_j + (1 - \frac{r}{2\Lambda})\delta ij]e^{-\frac{r(\tau)}{\Lambda}} \tag{27}$$

or in the algebraic form

$$\begin{aligned} R_{11} &= u^2[\frac{1}{2r\Lambda}\xi^2 + (1 - \frac{r}{2\Lambda})]e^{-\frac{r(\tau)}{\Lambda}} \\ R_{22} &= u^2[\frac{1}{2r\Lambda}\eta^2 + (1 - \frac{r}{2\Lambda})]e^{-\frac{r(\tau)}{\Lambda}} \\ R_{12} &= u^2[\frac{1}{2r\Lambda}\xi\eta]e^{-\frac{r(\tau)}{\Lambda}} \end{aligned} \tag{28}$$

By taking numerical Fourier transformations of the time domain correlation function (equation (27)), one obtains the frequency spectrum of the velocity correlation function, $G_{ij}(\omega)$, as

$$G_{ij}(\omega) = \frac{1}{2\pi} \int_{-\infty}^{\infty} R_{ij}(\tau) e^{-i\omega\tau} d\tau \tag{29}$$

where the omitted superscripts are the indices of two points for convenience.

In examining equation (26), it is clear that R_{ij} is periodic with respect to blade rotation due to the presence of the cosine term in the correlation function. This periodic term is most dominant when V/Ω is small. As τ or V increases, the importance of the cosine term decreases and R_{ij} becomes a monotonically decreasing function of τ. The spectrum represented by equation (29) should thus contain both a broadband and a blade rate hump spectrum in general. It resembles the experimental measurements and will be discussed in detail in the results section.

Sevik [1] and Martinez [8] studied special cases of the above equation. Sevik [1] considered the case where ΩR is much smaller than V and he approximated equation (26) by

$$r(\tau = 0) \equiv \sqrt{r_\alpha^2 + r_\beta^2 - 2 r_\alpha r_\beta \cos(\theta_\alpha - \theta_\beta)} \tag{30}$$

The corresponding velocity correlation then becomes

$$R_{ij} \simeq e^{-\frac{r(\tau=0)}{\Lambda}} R_{ii}(V\tau) \tag{31}$$

The components of the velocity correlation tensor are

$$R_{11} = u^2 e^{-(\frac{V\tau}{\Lambda} + \frac{r(\tau=0)}{\Lambda})} \tag{32}$$

and

$$R_{22} = u^2(1 - \frac{V\tau}{2\Lambda})e^{-(\frac{V\tau}{\Lambda}+\frac{r(\tau=0)}{\Lambda})} \tag{33}$$

The effect of the angular location of the blade, $\Omega\tau$, is totally absent in Sevik's correlation model; $e^{-r(\tau=0)/\Lambda}$ is a time independent term. The solution for G_{ij} contains no blade humps and may be expressed analytically; that is,

$$\begin{aligned} G_{11} &= \frac{2}{\pi}u^2\frac{\frac{V}{\Lambda}}{(\frac{V}{\Lambda})^2+\omega^2}e^{-r/\Lambda} \\ G_{22} &= \frac{2}{\pi}u^2\frac{\frac{V}{\Lambda}}{(\frac{V}{\Lambda})^2+\omega^2}(1 - \frac{1}{2}\frac{(\frac{V}{\Lambda})^2-\omega^2}{(\frac{V}{\Lambda})^2+\omega^2})e^{-r/\Lambda} \end{aligned} \tag{34}$$

Hoping to recover the blade rate humps without losing the simplicity of the analysis, Martinez [8] modified Sevik's analysis by including the propeller rotational speed through the approximation

$$r(\tau) \cong \sqrt{r_\alpha^2 + r_\beta^2 - 2r_\alpha r_\beta \cos(\theta_\alpha - \theta_\beta + \Omega\tau)} \tag{35}$$

Then the velocity correlation function becomes

$$R_{11} = u^2 e^{-(\frac{V\tau}{\Lambda}+\frac{r(\tau)}{\Lambda})} \tag{36}$$

and

$$R_{22} = u^2(1 - \frac{V\tau}{2\Lambda})e^{-(\frac{V\tau}{\Lambda}+\frac{r(\tau)}{\Lambda})} \tag{37}$$

which still preserves the exponential form of the correlation function used by Sevik [1]. The analytical form of the corresponding spectrum is given by Martinez in reference [8]. The solution contains Bessel functions. The modification of Martinez made the solution more complex and still did not recover the blade rate humps as he expected. As is true for the spectrum approach, simplification of the correlation function implies a filtering process in the physics. For practical applications, the search for an analytical solution could have prevented the advancement of unsteady force prediction methods in the past. The present analysis adapts both theoretical and numerical techniques. For individual cases, the theoretical analysis will be carried to its full extent, in this case to equation (29), and then numerical analysis will follow.

Fluid Dynamic Response Function - $H(\omega)$

The next step of the computation is the establishment of a transfer function, $H(\omega)$, defined in equation (16). The simplest computation is based on two-dimensional, incompressible and inviscid aerodynamics theory. Sears [10] derived the response function for a zero skew, discrete sinusoidal gust convected in the plane of a foil at zero angle of attack. The resulting aerodynamic unsteady force is represented as

$$H(\omega) = 2\pi\rho U \frac{C}{2} K(\omega) \tag{38}$$

where $K(\omega)$ is the Sears' function and is in terms of cylindrical functions $H_0^{(2)}(k)$ and $H_1^{(2)}(k)$;

$$K(\omega) = \frac{H_1^{(2)}(k)}{H_1^{(2)}(k) + iH_0^{(2)}(k)} \tag{39}$$

where k is the normalized reduced frequency ($\omega C/2U$).

Equation (38) was derived for an isolated foil operating with sinusoidal velocity disturbances normal to the foil surface. When applying the equations to propellers or small aspect ratio foils, the results of using a two-dimensional approximation may not valid. However, the two-dimensional theory will give satisfactory predictions providing the value of the local lift slope is appropriately corrected. This means that the coefficient 2π of equation (38) be replaced by the steady state local lift slope as described by Sevik [1].

Applying the above Sears' function to a two-dimensional blade, the angle between the inflow and the direction of advance also has to be considered. This gives

$$H_p(\omega) \;=\; H(\omega)\cos\phi \tag{40}$$

where H_p denotes the two-dimensional response function for a propeller in its direction of advance and ϕ is the inflow angle with respect to that direction. When operating near design conditions, ϕ may be approximated by the pitch angles of blade sections for most marine propellers.

Numerical Procedures

With a specified correlation function, equation (28), and a chosen transfer function, equation (40), we may proceed to perform the numerical unsteady force computations as given in equation (16). Since propeller unsteady forces are generated from the unsteady velocity relative to the

blades, the velocity spectrum components $G(\omega)$ in equation (16) should be expressed in a rotational cylindrical coordinate system which is fixed on the blade. Let the mean inflow to the propeller be denoted by $\overline{u^\alpha}$. Then the unsteady angle of attack becomes

$$\begin{aligned} \alpha(\tau) &\simeq \tan^{-1} \frac{u_N^\alpha}{\overline{u^\alpha}} \\ &\simeq \frac{u_N^\alpha}{\overline{u^\alpha}} \end{aligned} \tag{41}$$

with

$$u_N^\alpha = u_x^\alpha \cos\phi_\alpha + u_\theta^\alpha \sin\phi_\alpha \tag{42}$$

and

$$\begin{aligned} u_N^\alpha u_N^\beta &= (u_x^\alpha(0)\cos\phi_\alpha(0) + u_\theta^\alpha \sin\phi_\alpha(0)) + (u_x^\beta \cos\phi_\beta(\tau) + u_\theta^\beta \sin\phi_\beta(\tau)) \\ &= u_x^\alpha u_x^\beta \cos\phi_\alpha(0)\cos\phi_\beta(\tau) + u_x^\alpha u_\theta^\beta \cos\phi_\alpha(0)\sin\phi_\beta(\tau) + \\ &\quad u_\theta^\alpha u_x^\beta \sin\phi_\alpha(0)\cos\phi_\beta(\tau) + u_\theta^\alpha u_\ell^\beta \sin\phi_\alpha(0)\sin\phi_\beta(\tau) \end{aligned} \tag{43}$$

where ϕ_α is the propeller inflow angle at point α and is defined in equation (39).

The velocity correlation of equation (16), thus, becomes

$$\begin{aligned} R_{NN}^{\alpha\beta} &= R_{xx}^{\alpha\beta}\cos\phi_\alpha(0)\cos\phi_\beta(\tau) + R_{x\theta}^{\alpha\beta}\cos\phi_\alpha(0)\sin\phi_\beta(\tau) + \\ &\quad R_{\theta x}^{\alpha\beta}\sin\phi_\alpha(0)\cos\phi_\beta(\tau) + R_{\theta\theta}^{\alpha\beta}\sin\phi_\alpha(0)\sin\phi_\beta(\tau) \end{aligned} \tag{44}$$

The calculation of $R_{xx}^{\alpha\beta}$ is straight forward as

$$R_{xx}^{\alpha\beta} = u^2[\frac{1}{2r\Lambda}dx^2 + (1 - \frac{r}{2\Lambda})]e^{-\frac{r(\tau)}{\Lambda}} \tag{45}$$

where $dx = V\tau$ and

$$r(\tau) \equiv \sqrt{(dx)^2 + r_\alpha^2 + r_\beta^2 - 2r_\alpha r_\beta \cos(\theta_\alpha(0) - \theta_\beta(0) + \Omega\tau)} \tag{46}$$

The calculations of $R_{x\theta}^{\alpha\beta}$ and $R_{\theta\theta}^{\alpha\beta}$ in terms of τ has to be further expressed through the instantaneous angular locations of the blade elements. For the coordinate system shown in Figure 5, the tangential velocity component is

$$u_\theta^\beta = u_y^\beta \cos\theta_\beta(\tau) - u_z^\alpha \sin\theta_\beta(\tau) \tag{47}$$

and the velocity correlations $R_{x\theta}^{\alpha\beta}$ and $R_{\theta\theta}^{\alpha\beta}$ are

$$R_{x\theta}^{\alpha\beta} = R_{xy}^{\alpha\beta} \cos\theta_\beta(\tau) - R_{xy}^{\alpha\beta} \sin\theta_\beta(\tau) \tag{48}$$

and

$$\begin{aligned} R_{\theta\theta}^{\alpha\beta}(\tau) = {} & R_{yy}^{\alpha\beta} \cos\theta_\alpha(0) \cos\theta_\beta(\tau) + R_{zz}^{\alpha\beta} \sin\theta_\alpha(0) \sin\theta_\beta(\tau) - \\ & R_{yz}^{\alpha\beta} \cos\theta_\alpha(0) \sin\theta_\beta(\tau) - R_{yz}^{\beta\alpha} \sin\theta_\alpha(0) \cos\theta_\beta(\tau) \end{aligned} \tag{49}$$

where

$$
\begin{aligned}
R_{yy}^{\alpha\beta} &= u^2[\frac{1}{2r\Lambda}dy^2 + (1 - \frac{r}{2\Lambda})]e^{-\frac{r(\tau)}{\Lambda}}, \\
R_{xy}^{\alpha\beta} &= u^2(1 - \frac{r}{2\Lambda}dxdy)e^{-\frac{r(\tau)}{\Lambda}}, \\
R_{xz}^{\alpha\beta} &= u^2(1 - \frac{r}{2\Lambda}dxdz)e^{-\frac{r(\tau)}{\Lambda}}, \\
R_{zz}^{\alpha\beta} &= u^2[\frac{1}{2r\Lambda}dz^2 + (1 - \frac{r}{2\Lambda})]e^{-\frac{r(\tau)}{\Lambda}}, \\
dy &= r_\alpha \cos\theta_\alpha(0) - r_\beta \cos\theta_\beta(\tau),
\end{aligned}
$$

and

$$
dz = r_\alpha \sin\theta_\alpha(0) - r_\beta \sin\theta_\beta(\tau).
$$

Since turbulence has been assumed to be homogeneous, $R_{\theta\theta}^{\alpha\beta}(\tau)$ is only a function of τ, and can be evaluated at $\theta_\alpha(0)$ and $\theta_\beta(\tau)$.

Based on the above definition of R_{NN}, correlation functions are numerically evaluated at given ω values as

$$
G_{NN}^{\gamma\delta}(\omega) \equiv \frac{1}{2\pi}\int_{-\infty}^{\infty} R_{NN}^{\gamma\delta}(\tau)e^{-i\omega\tau}d\tau \tag{50}
$$

The thrust spectrum tensor, equation (16), between blade elements α and β is then calculated as:

$$
\Psi_{\ell_x\ell_z}^{\alpha\beta}(\omega) = [H_{xx}^{\alpha\gamma}(\omega)]^*[H_{xx}^{\beta\delta}(\omega)][G_{11}^{\gamma\delta}(\omega)] \tag{51}
$$

Assuming the unsteady force generated at each individual strip is two dimensional, the last equation becomes

$$\Psi^{\alpha\beta}_{\ell_x\ell_x}(\omega) \;=\; [H_p^{\alpha\alpha}(\omega)]^*[H_p^{\beta\beta}(\omega)][G^{\alpha\beta}_{NN}(\omega)]$$

with H_p given by equation (39). The total unsteady force spectrum is obtained from summing $\Psi^{\alpha\beta}_{\ell_1\ell_1}(\omega)$ over all elements of α and β. In this computation, the mean flow angle ϕ has to be estimated before the unsteady thrust can be determined. This angle can be obtained from propeller computer codes. For near-design operating conditions, the pitch of the blade may be used for ϕ for most marine propellers, as mentioned earlier.

Results and Discussions

Sevik's experiment [1] is used to study the present approach and to demonstrate the differences between the present computation and previous results. The experiment was conducted in the 1.22m (48") diameter water tunnel at Pennsylvania State University. The propeller used for this investigation has ten blades with a constant chord length of 2.54cm (1") and a radius of 10.16cm (4"). The turbulence level in the test section without the grid was about 0.1%. Two grids were used with mesh sizes of 10.16cm (4") and 15.24cm (6"), respectively, to generate the turbulence level of about 3% with two different integral length scales at the propeller plane. The distance between the grid and the propeller plane was twenty times the grid sizes. Data were taken at a tunnel speed equal to 4.57m/sec (15ft/sec) and the advance ratio was 1.22. Power spectral density of the propeller thrust due to turbulence was measured and compared with theoretial results of Sevik [1], Figure 6. The measured spectra show significant humps at the first blade rate frequency while the humps at the higher blade rates were observable only for the 15.24cm grid case. The theoretical results of Sevik compared well with the measurements with respect to the broadband part of the spectrum while the humps were missing. Later, Blake [7] compared those data with his asymptotic solutions of equation

(12) and equation (13), derived to improve the prediction on blade rate humps. His results are also given in Figure 6. The smooth broken line in Figure 6 shows the asymptotic results of small correlation (equation (12)) and the dotted line provides the large correlation results (equation (13)). It is seen that the small correlation results approach Sevik's theory as expected since they are equivalent to omitting the rotational correlation from the analysis. The large correlation asymptotic results give humps centered at multiples of the blade rate frequency without the broadband part of the spectrum. The comparison of the asymptotic solutions and measurement indicate that the basic approach is correct and that numerical simplification should be avoided.

Computations based on equation (10) and equation (11) were performed numerically for the two grid sizes, and the results are given in Figures 7 and 8. The results of equation (11), Figure 7, show that the center frequencies of the humps shift and skew to higher frequencies when compared with Blake's calculations. The amplitudes of the humps do not decay at higher blade rates for either grid size. Also, the results using equation (11) show ditches between the humps quite below the measured results. Since equation (11) did not have the radial dependence of the filtering function, A_s, Sears' function and Taylor's hypothesis, it over emphasizes the blade rotational effect. By removing the small advance coefficient assumption, including the radial dependence on filtering and Sears' functions, and numerically integrating equation (10), the hump amplitude and ditch depth are reduced and the hump bandwidth is increased as shown in Figure 8. It is thus demonstrated, in a practical application, that the radial dependence should be included in the analysis. Neverthless, including this effect in the wave number integration complicates the computation and the spectrum approach is not recommended at present.

Figures 9a and 9b present the comparisons between the results of the present correlation theory and the experiment. The current correlation theory predicts both the humps which were demonstrated in the experiment and the broadband part of the spectrum. The broadband part of the

spectrum compares well while the hump amplitudes and center frequencies of higher harmonics do not agree. The cause of the hump discrepancy could be in the uncertainty of the inflow turbulence. The experiments show the inconsistency in the results between10.16cm (4") and 15.24cm (6") grids. The 15.24cm (6") grid results have humps at both first and second blade rate frquencies while 10.16cm (4") grid results show only one hump near the first blade rate. These differences could reflect deviations from the design homogeneous and isotropic grid turbulent inflow. Since the characteristics of the inflow were not measured, no further comparisons are possible. However, from the general features of the comparsion and the other computations which are not included, the authors are certain that the present model should predict the spectrum reasonably well if the inflow turbulence is given.

The characteristics of the unsteady force spectrum may be generalized from the study of isotropic turbulence. The present isotropic results show that the spectrum can be normalized in terms of the parameters $V/\Lambda\Omega, \Lambda/R$ and ω/Ω. Their influence on the resulting unsteady force is demonstrated in Figures 10 and 11, and is summarized as follows:

1) The effect of the inflow turbulence scale, Λ/R: In general, the smaller the turbulence length scale, the higher the broadband unsteady spectrum. However, both amplitudes and bandwidths of the blade rate humps decrease with decreasing turbulence scale as the result of faster decay of the rotational correlations, while the variation of the turbulence length scale has only a minimal effect on the hump center frequencies, Figure 10.

2) The effect of advance coefficient, $V/\Lambda\Omega$: With other nondimensional parameters held constant, Figure 11 shows that as the advance coefficient decreases, the blade rate humps become more pronounced. The higher blade rate humps become significant at low advance coefficients as shown by Blake[7] and discussed previously. In the normal operating condition ($V/\Lambda\Omega$ greater than 0.5), only the first blade rate hump is expected.

3) Skew of the hump center frequencies: The center frequencies of the humps shown in Figure 12 are not at blade rate frequencies and are skewed

to the right. The skew is caused by the geometrical pitch of the blade. The larger the pitch, the greater the skew will be. The first order estimate of this skewness may be approximated from equations (11) or (48).

4) Inverse cubic dependency on the high frequencies: To demostrate the spectrum behavior at high frequencies, the theoretical results of the grid turbulence for 10.16 cm and 15.24 cm screens are re-plotted in normalized form in Figure 13. The frequency is normalized by the blade rate frequency and the thrust spectrum is normalized by the third power of the velocity. At high frequencies, past the second hump, the slope of these normalized curves approaches minus three as expected from equation (12) or equations (34) and (38) for a given advance coefficient and turbulence level. The two grids used in the experiment did not cover enough of a range in turbulence lengths to make as substantial alterations near the hump as the theoretical calculation provided in Figure 10.

Because ships normally operate at a nearly constant advance coefficient, it is of interest to present the thrust spectrum in dimensional form as a function of ship speed or propeller rpm with a given advance coefficient. The behavior of the thrust spectra at different speeds for the 10.16 cm grid turbulence is shown in Figure 14. It is seen that the hump bandwidth at the first blade rate frequency increases as ship speed increases. In practice, one should anticipate a sharp hump during lower speed operation.

Conclusions

Theoretical predictions of broadband thrust forces in a turbulent flow are presented. The calculations are carried out using a correlation method and a spectrum method. The results of the correlation theory provide a better correlation with experiment than the spectrum theory, computed from an assumption of homogeneous and isotropic turbulence. Turbulence velocity correlation can be considered as the combination of transverse and rotational correlation. The effect of transverse correlation produces

an unsteady thrust proportional to the third power of ship speed. The rotational correlation is inversely proportional to a rotational parameter given by $V/\Lambda\Omega'$. The rotational correlation distorts the V^3 power relation and causes the unsteady thrust spectra to show humps near the first and second blade rate frequencies; these humps skew to the higher frequency side of the blade rate frequencies. Since the hump phenomena were not explained previously, only limited, inconclusive experiments are available to verify the theory. Future experiments should include simultaneous measurement of unsteady force and turbulence in order to validate the theory.

The spectrum method is not as easy to apply as the correlation method because it involves higher order integration. When the integration order was reduced through simplification, the results were also degraded as shown in Figures 6 through 8. The correlation method gives good results, Figure 9, and can be adapted to more complex cases with little numerically difficulty.

In addition to improving the inflow turbulence assumptions, the analytical methods can be further improved by including the effect of finite span, camber and angle of attack. A parametric investigation of the turbulence inflow and propeller unsteady response should be done under laboratory conditions before the theory is applied to a complex propeller/rotor geometry.

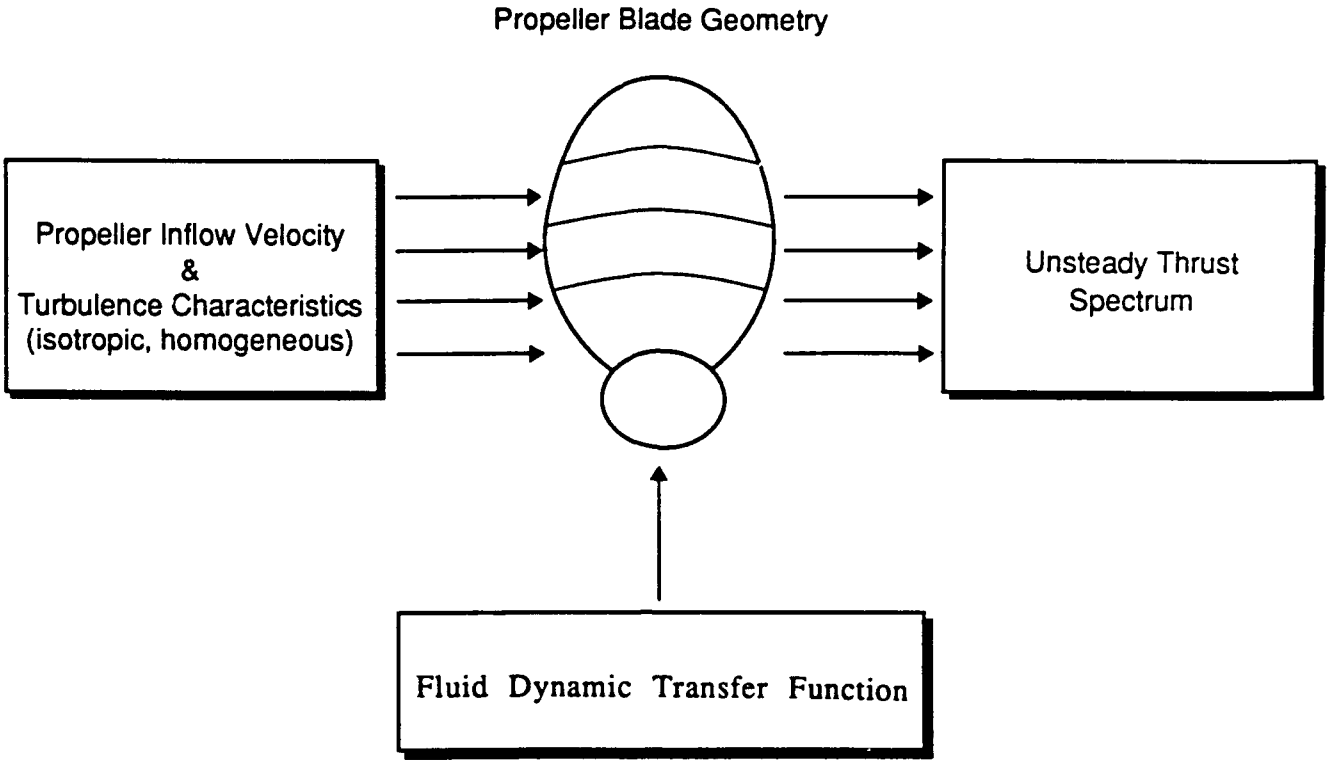

Fig. 1. Flow chart of excitation force model.

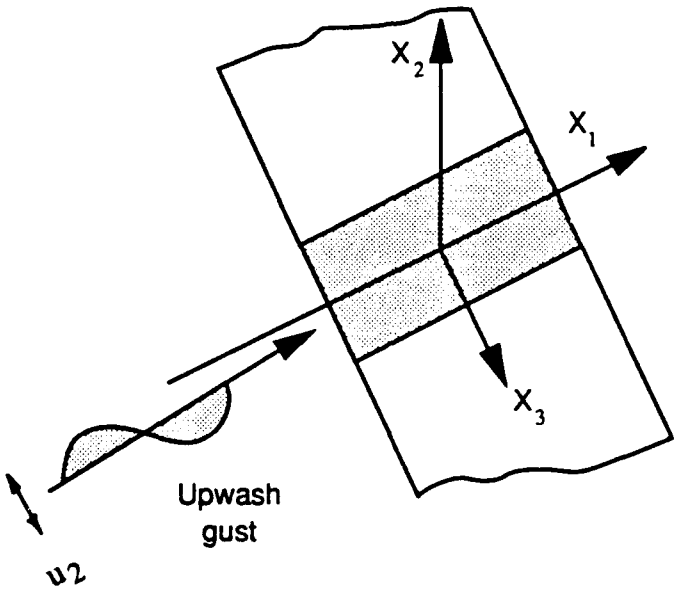

Fig. 2. Definition of local coordinate system.

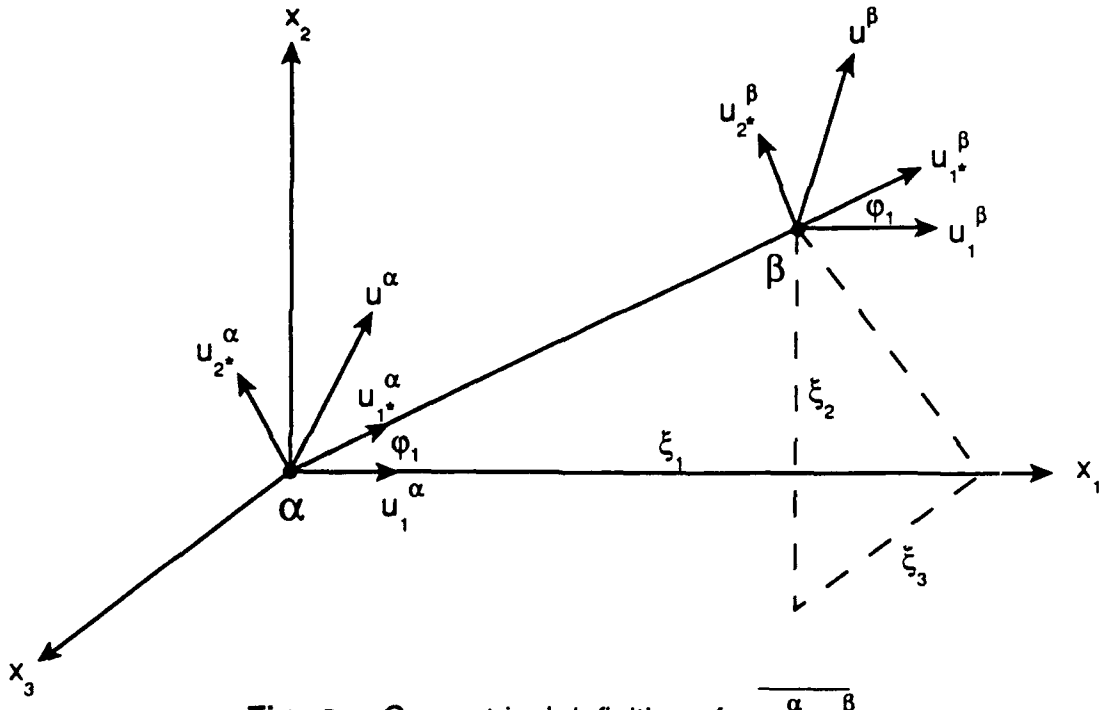

Fig. 3. Geometrical definition of $\overline{u_1^{\alpha} u_1^{\beta}}$.

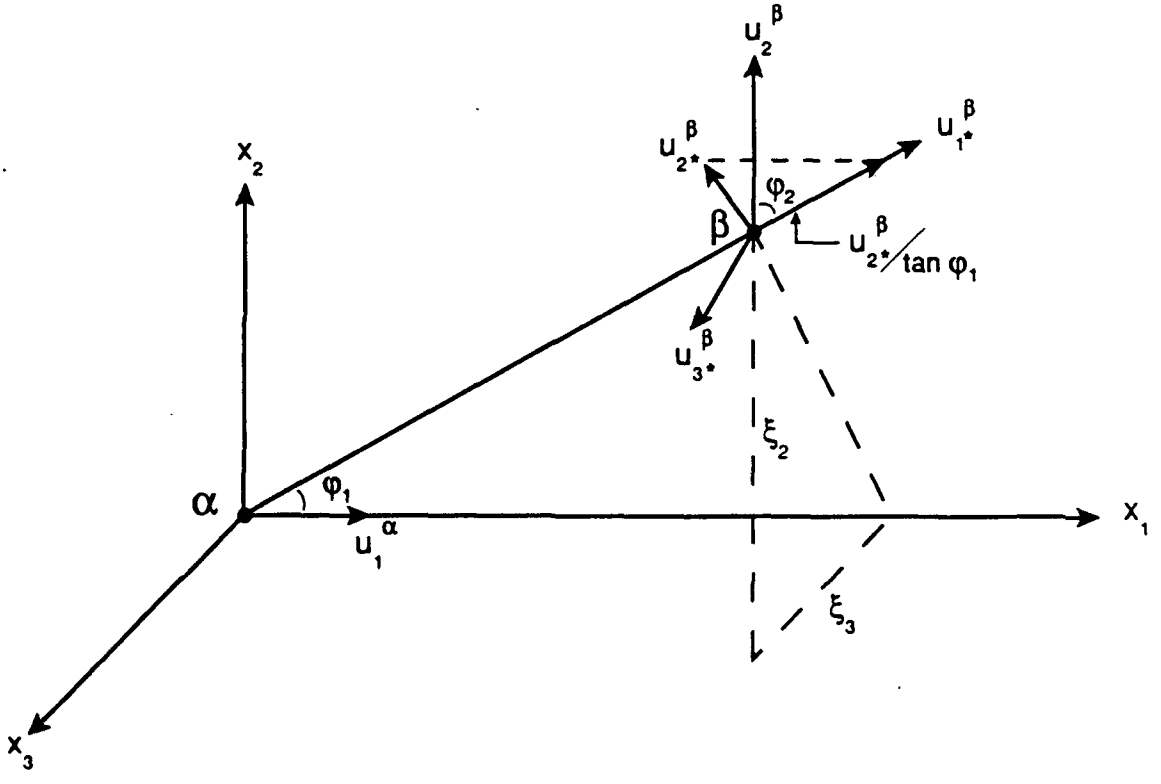

Fig. 4. Geometrical definition of $\overline{u_1^{\alpha} u_2^{\beta}}$.

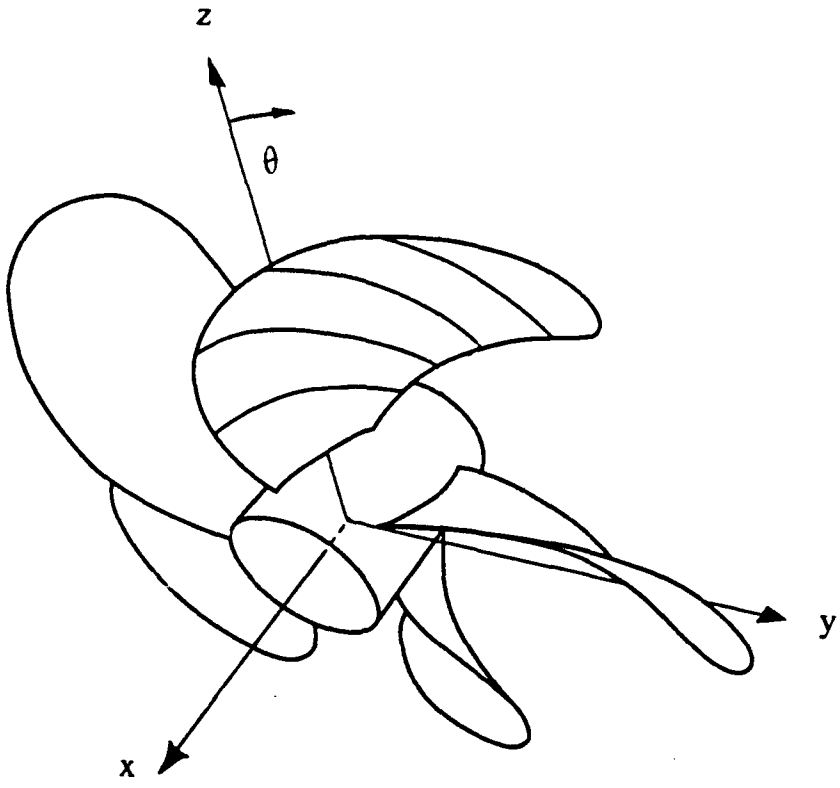

Fig. 5. Chordwise strips on propeller blade.

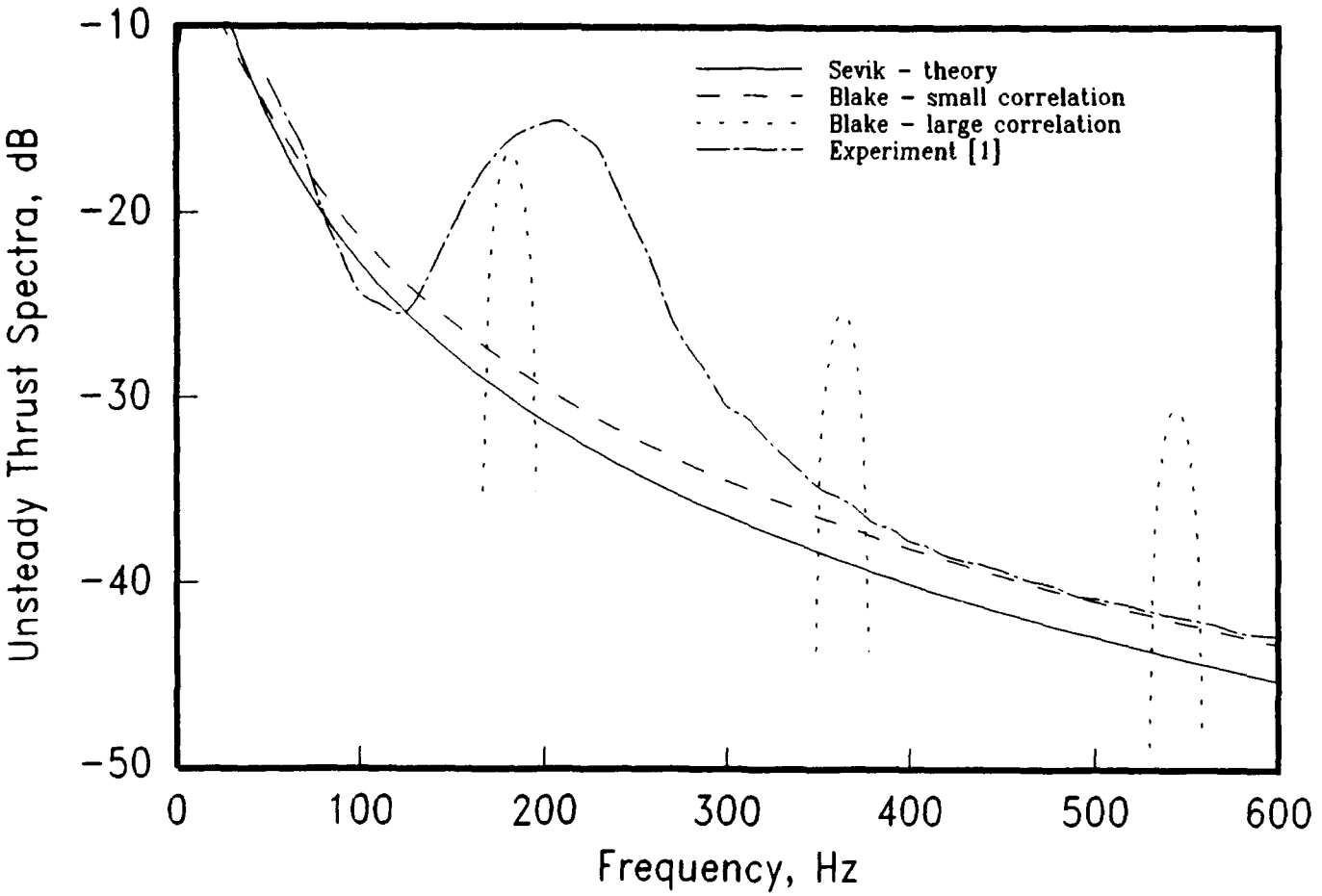

Fig.6a 10.16cm Grid

Fig.6 Comparison of Existing Methods

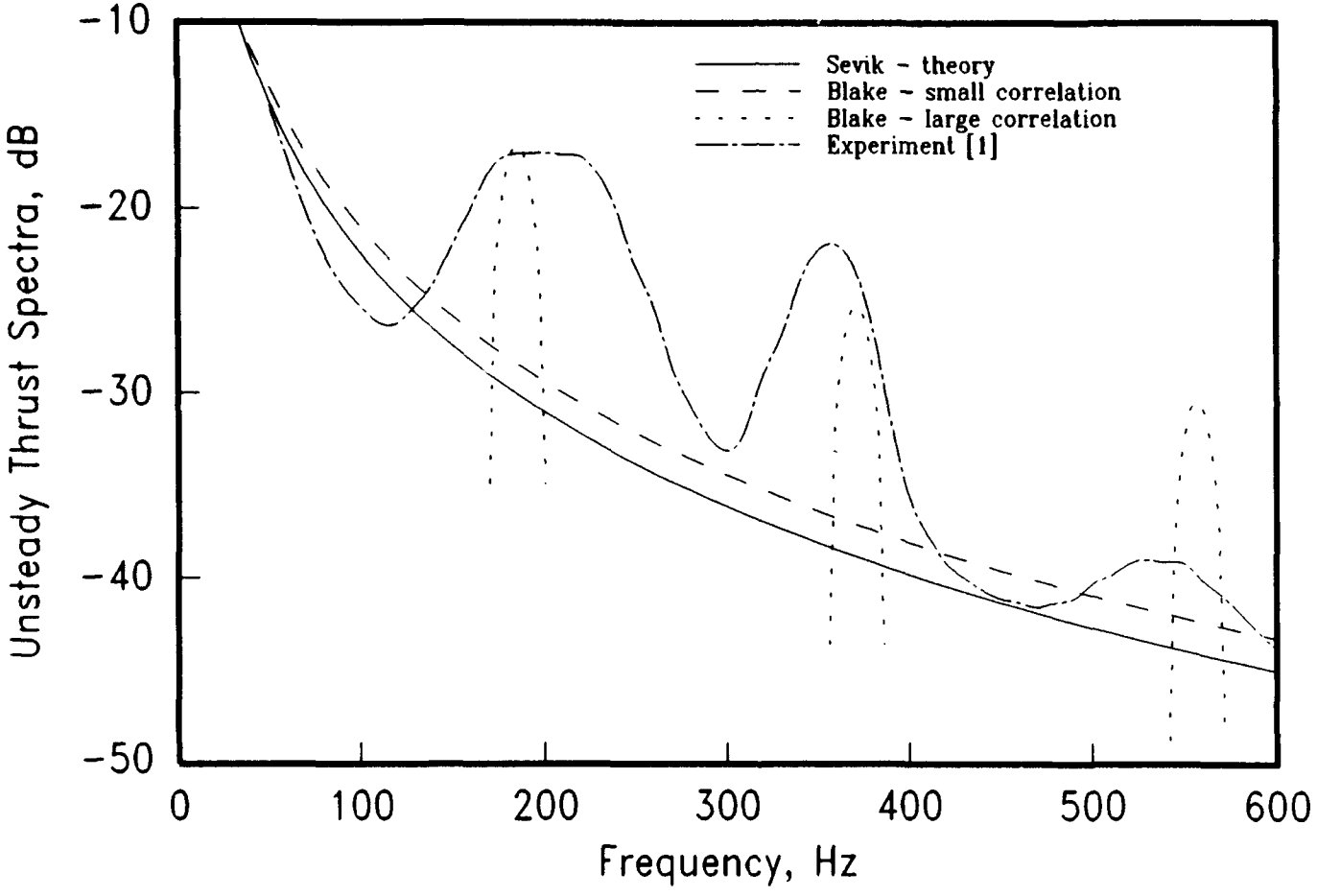

Fig.6b 15.24cm Grid

Fig.6 (Continued)

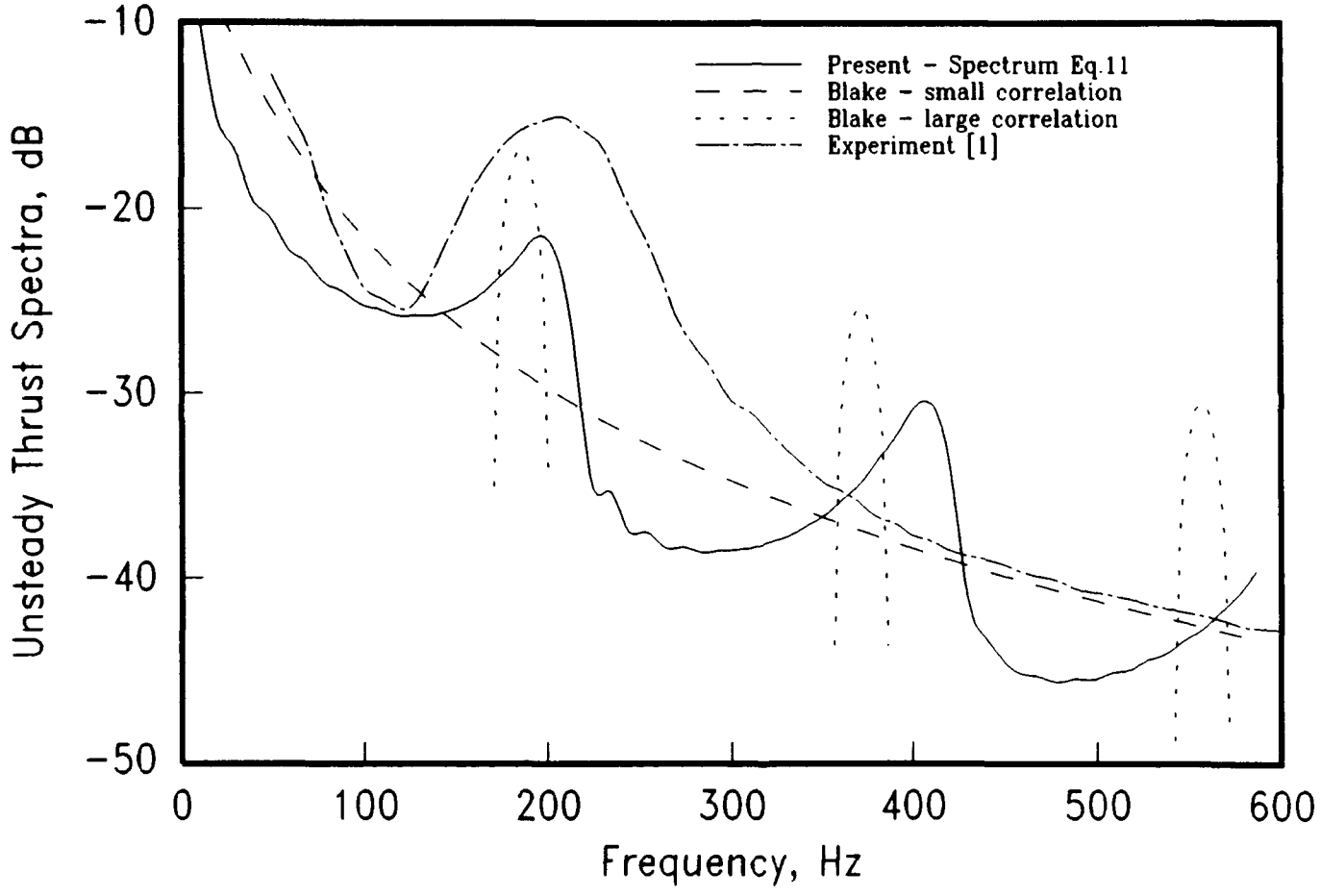

Fig.7a 10.16cm Grid

Fig.7 Comparison of Simplified Spectrum Approaches

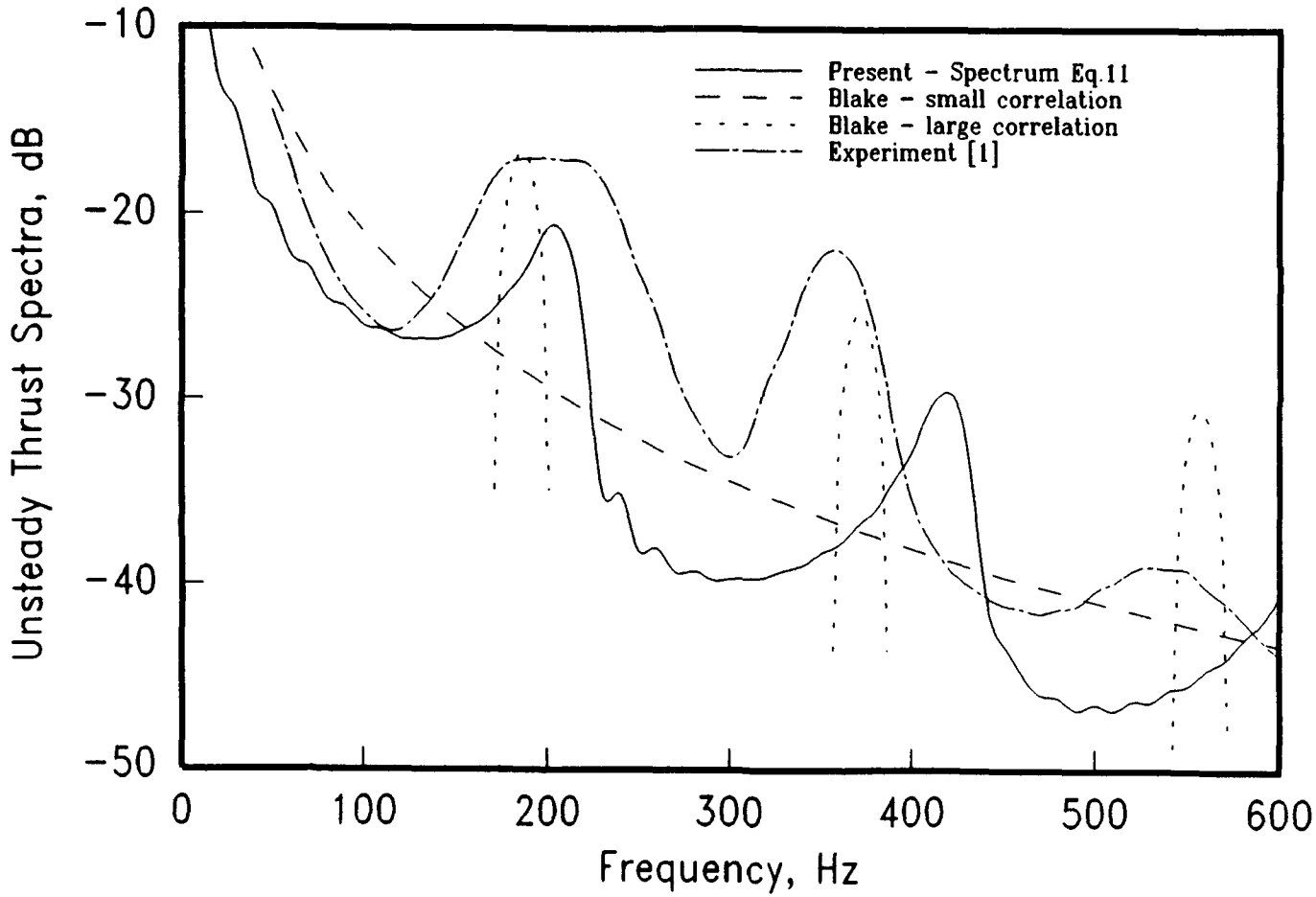

Fig. 7b 15.24cm Grid

Fig.7 (Continued)

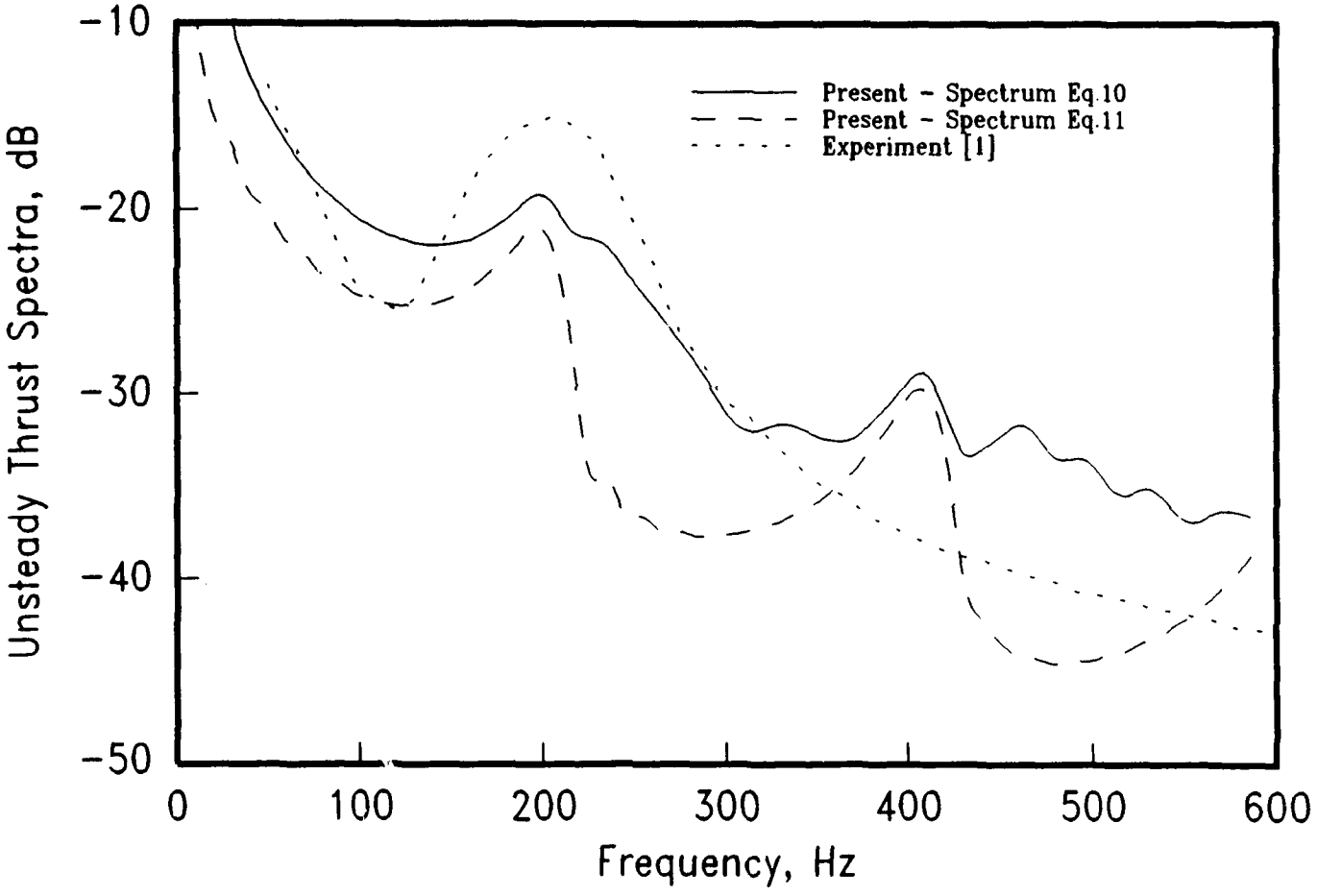

Fig.8a 10.16cm Grid

Fig.8 Comparison of Unified Spectrum Methods with Experiment

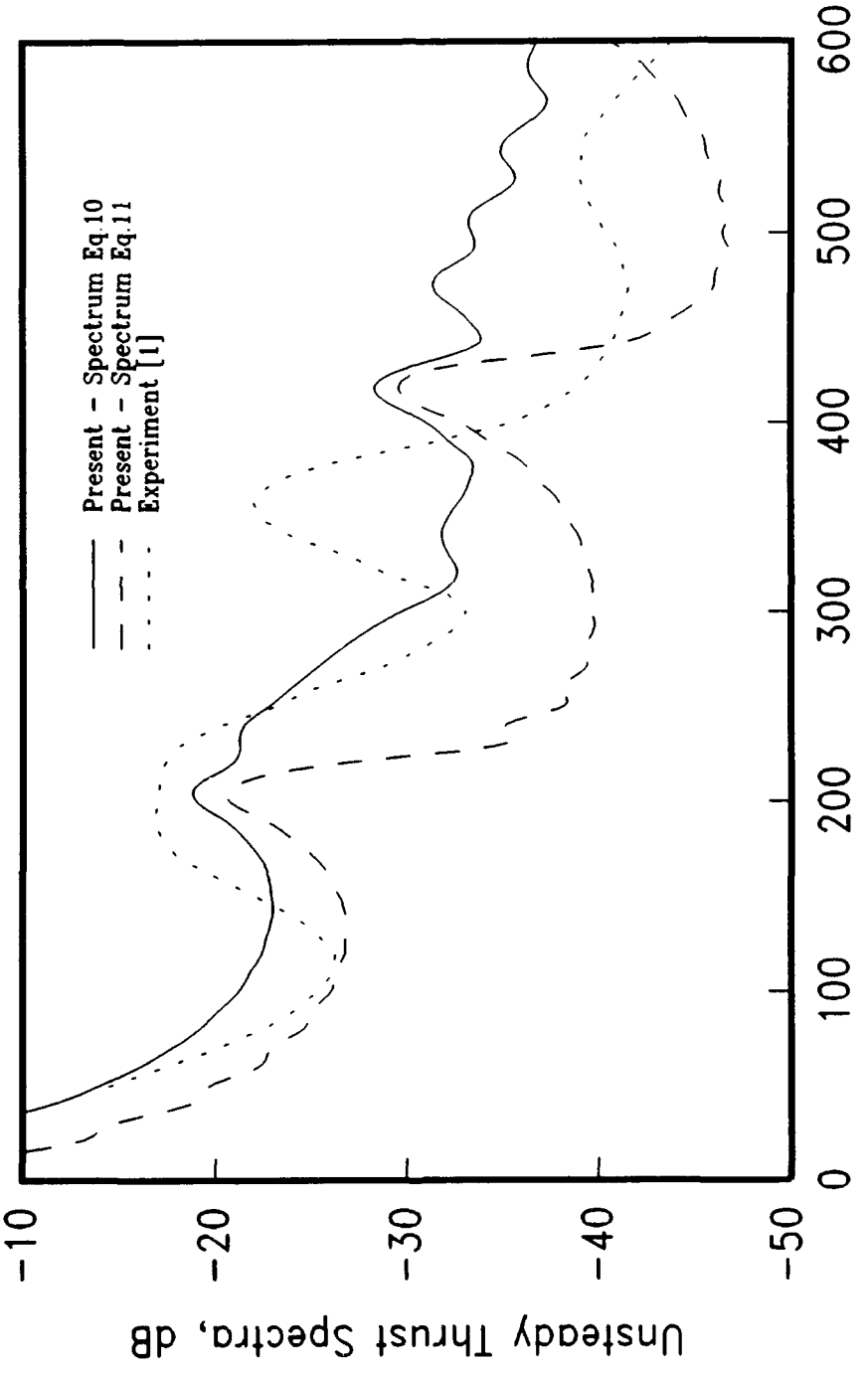

Fig.8b 15.24cm Grid

Fig.8 (Continued)

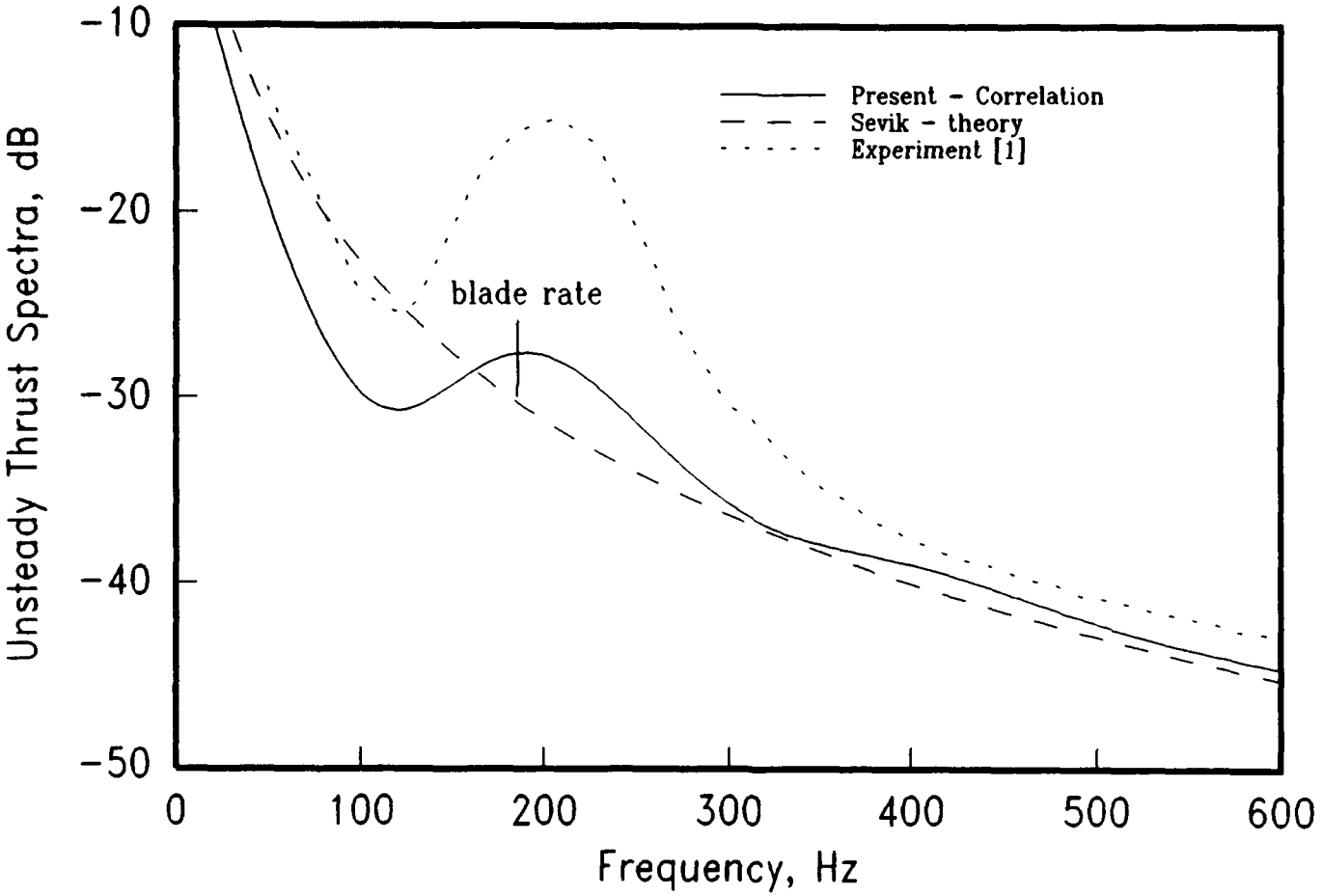

Fig.9a 10.16cm Grid

Fig.9 Comparison of Correlation Methods With Experiment

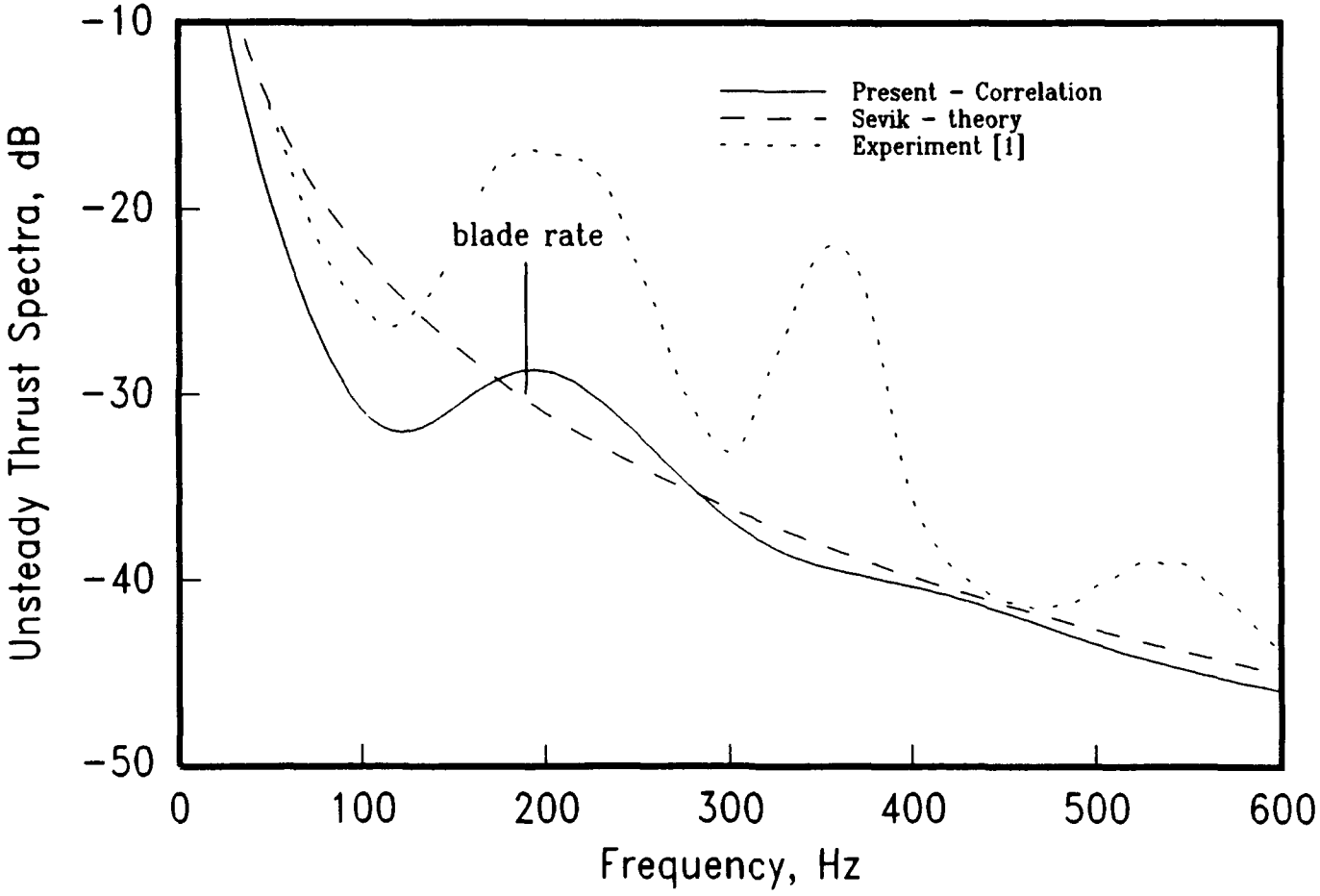

Fig.9b 15.24cm Grid

Fig.9 (Continue)

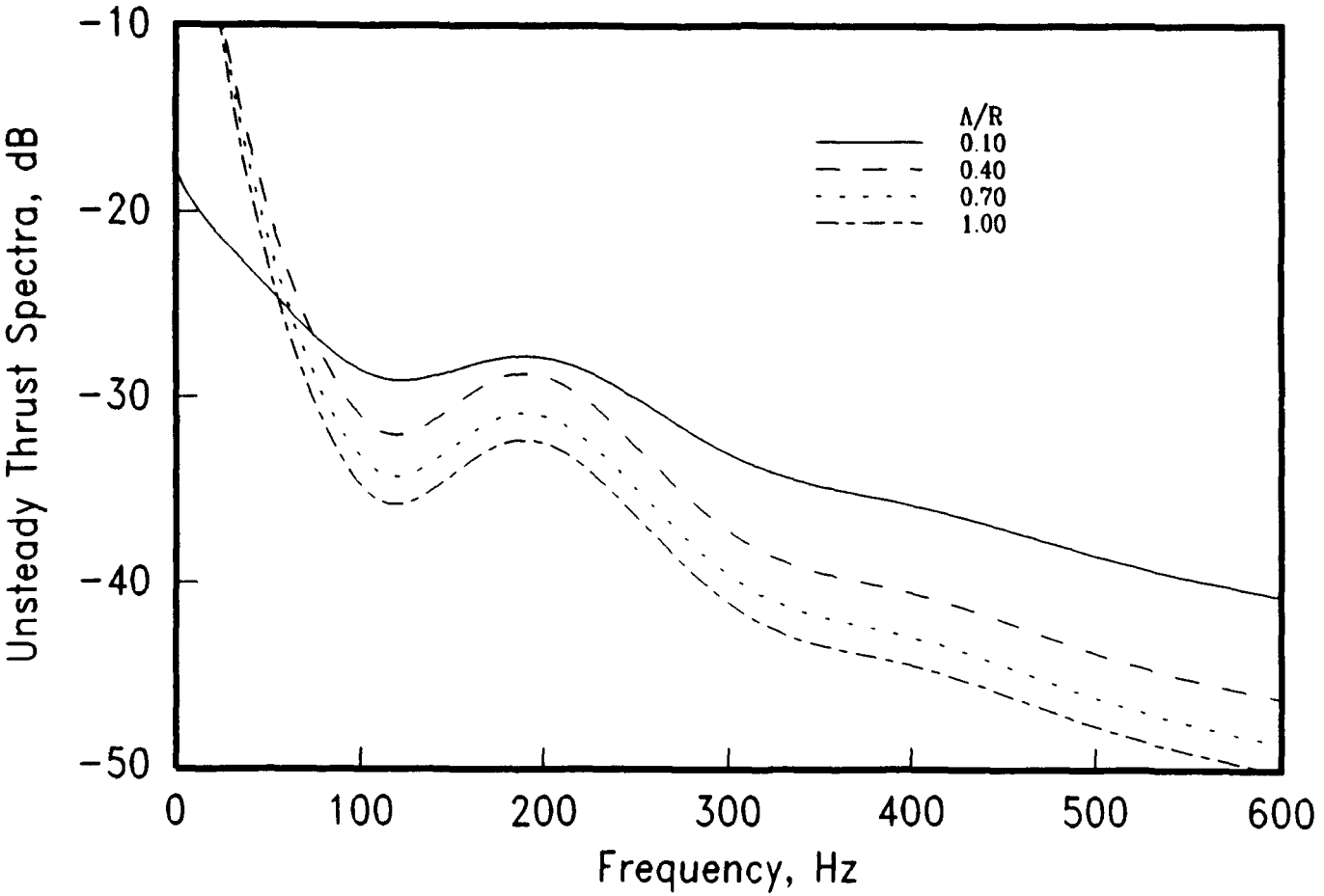

Fig.10 Effect of Turbulence Length Scale (Λ/R) on Unsteady Thrust

(Turbulence Level = 0.03; V/RΩ=0.39)

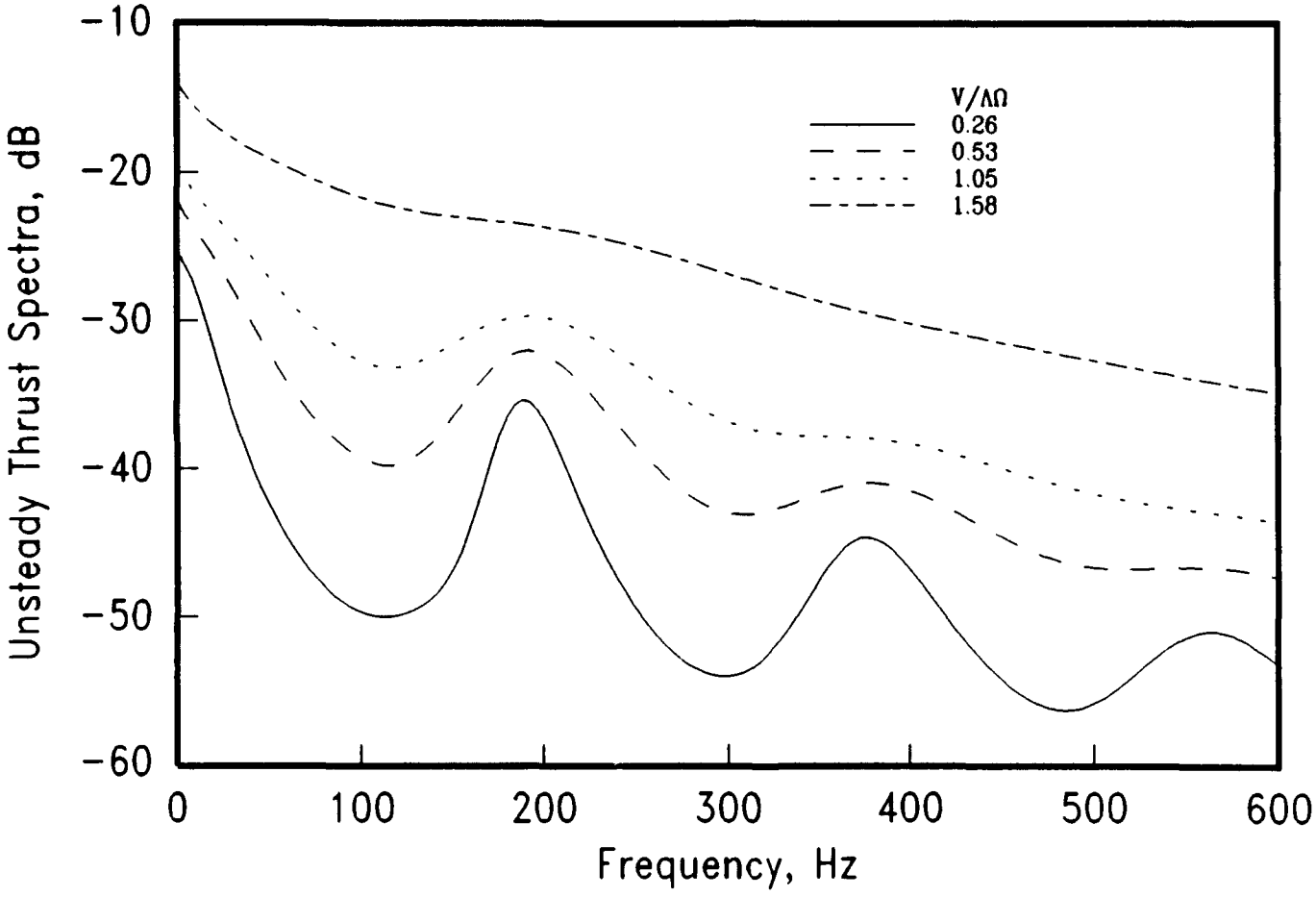

Fig.11 Effect of Advance Coefficient ($V/\Lambda\Omega$) on Unsteady Thrust (Turbulence Level = 0.03; Λ/R=0.28)

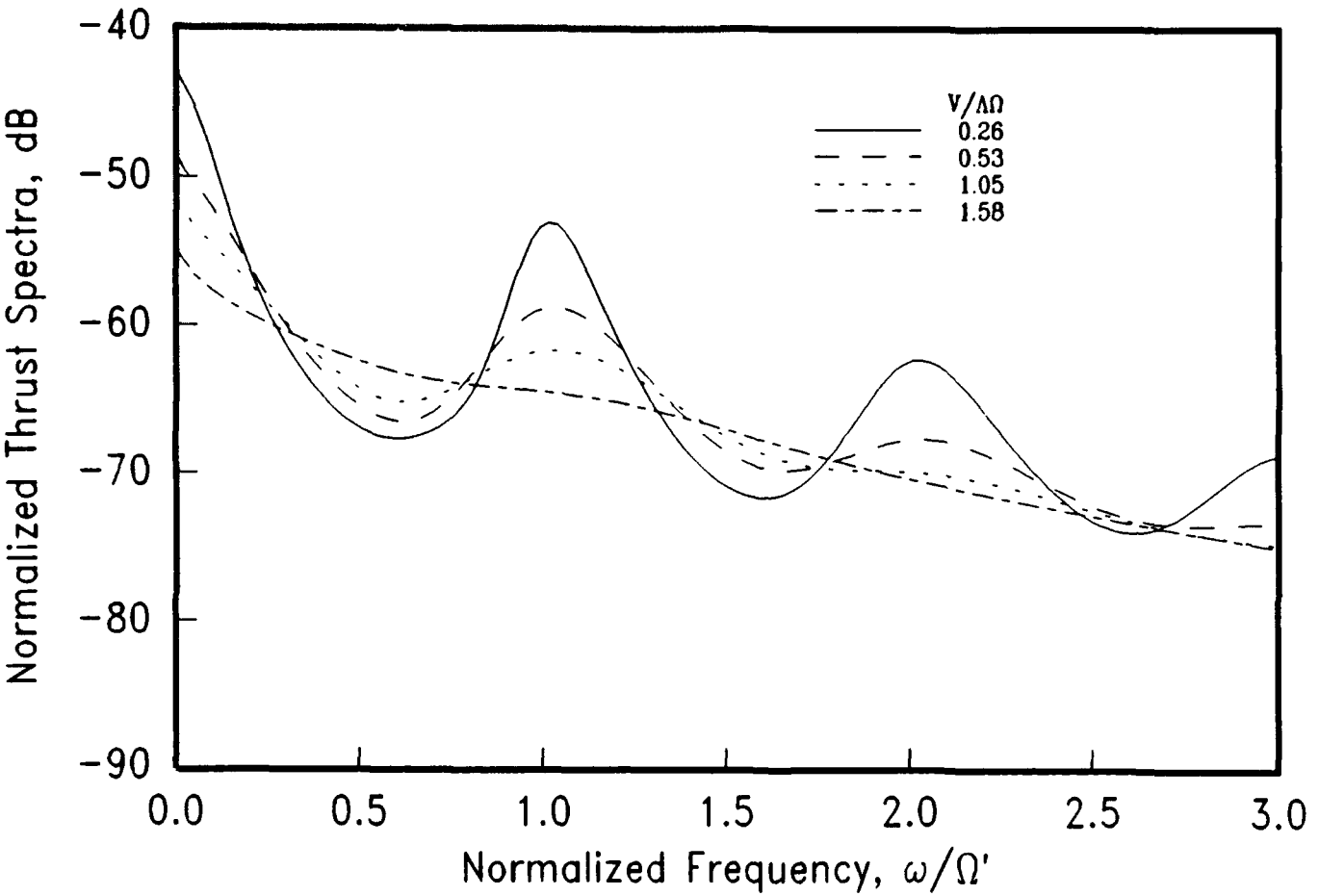

Fig.12 Normalized Effect of Advance Coefficient ($V/\Lambda\Omega$) on Unsteady Thrust (Turbulence Level = 0.03; Λ/R=0.28)

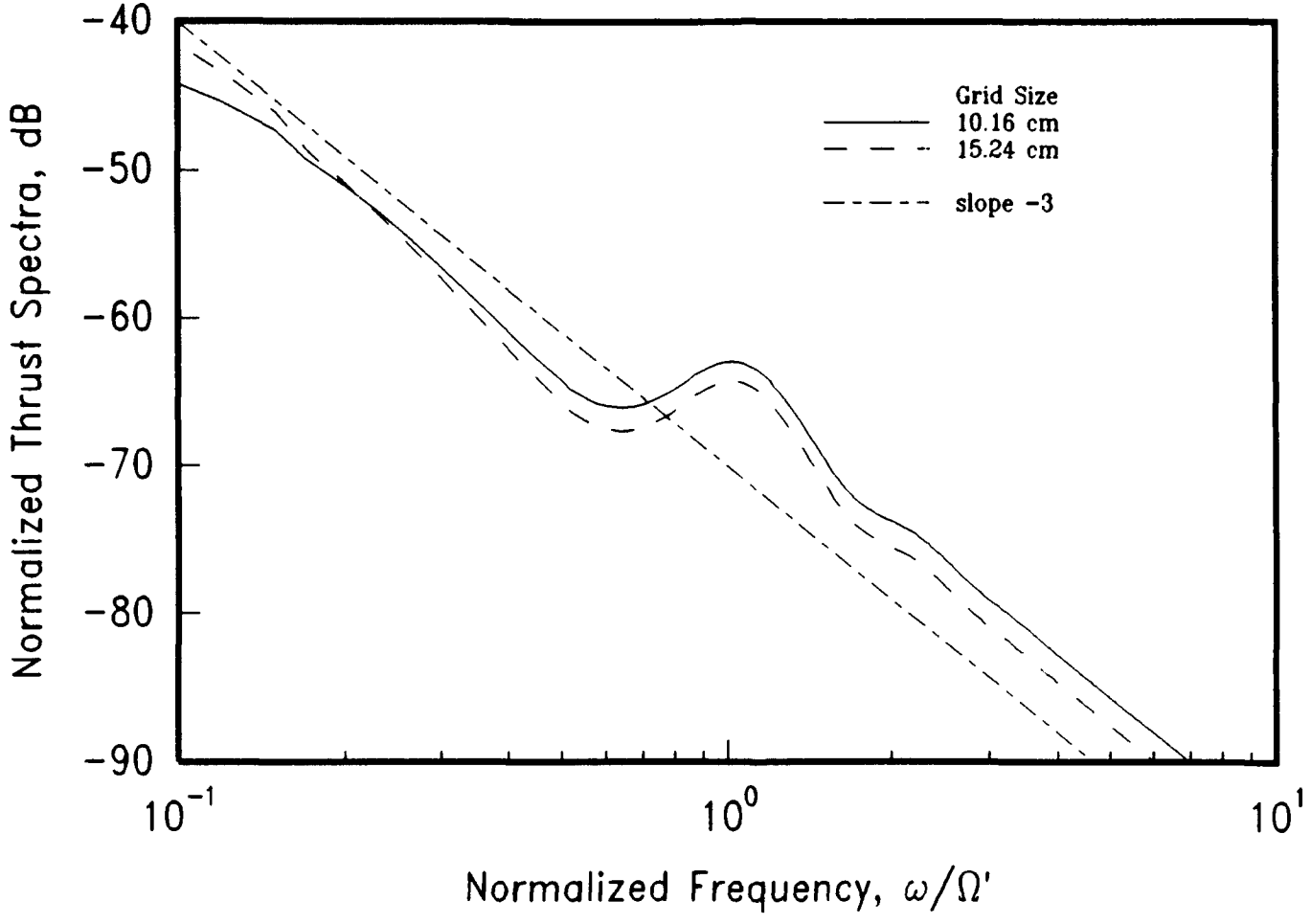

Fig.13 Normalized Unsteady Thrust
(Turbulence Level = 0.03; J=1.22)

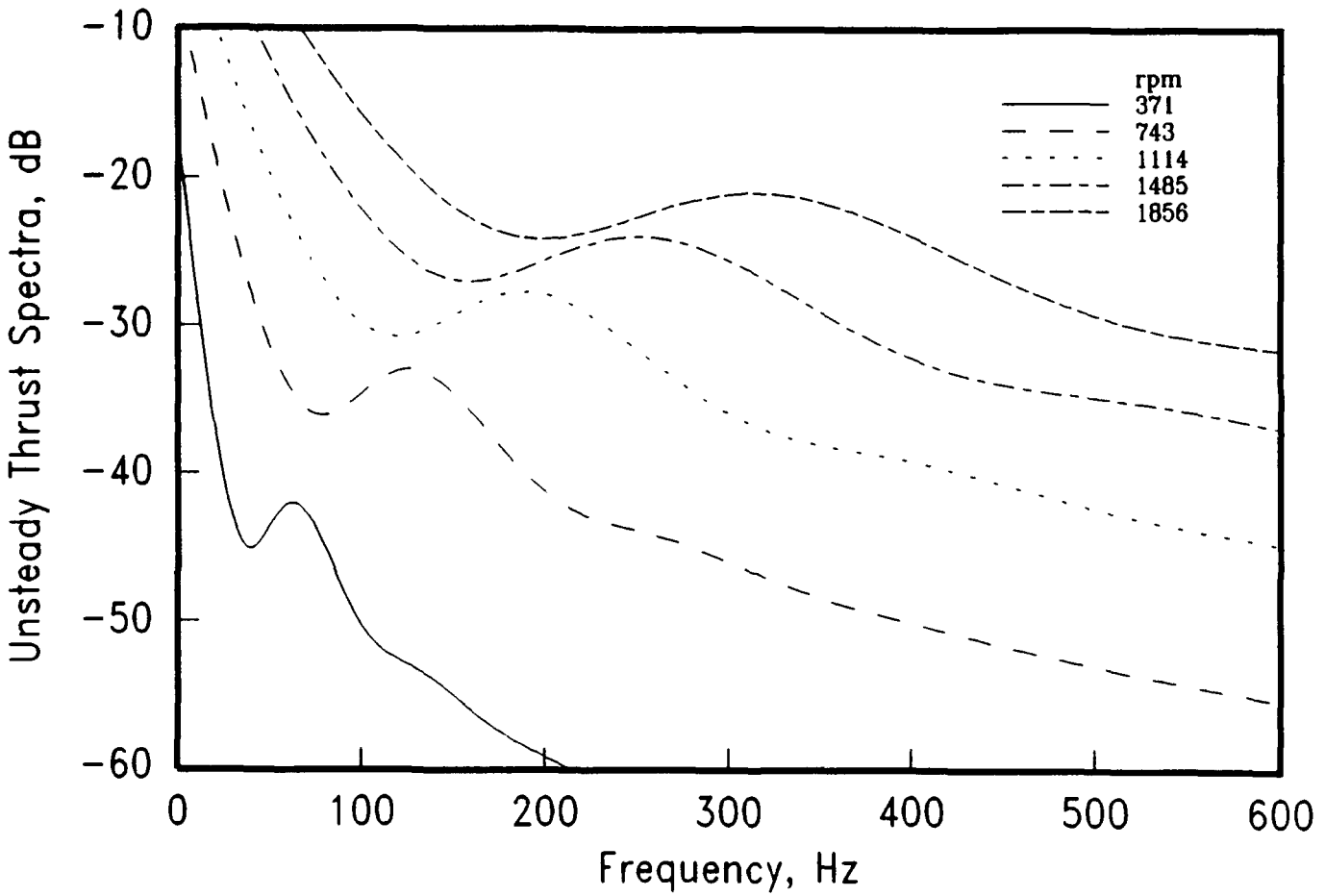

Fig.14 Unsteady Thrust at Constant Advance Coefficient

(Turbulence Level = 0.03; 10.16cm Grid, J=1.22)

References

1. Sevik, M., "Sound Radiation From a Subsonic Rotor Subjected to Turbulence," Int. Symp. Fluid Mech. Des. Turbomach., Pennsylvania State University, University Park; NASA SP-304, Part II (1974).

2. Thompson, D. E., "Propeller Time-Dependent Forces Due to Nonuniform Flow," PhD Thesis, The Pennsylvania State University, May 1976.

3. Chandrashekhara, N., "Tone Radiation From Axial Flow Fans Running in Turbulent Flow," J. Sound Vib., 18,533-543 (1971).

4. Mani, R., "Noise Due to Interaction of Inlet Turbulence With Isolated Stators and Rotors," J. Sound Vib., 17,251-260 (1971).

5. Homicz, G. F., and George, A. R., "Broadband and Discrete Frequency Radiation From Subsonic Rotors," J. Sound Vib., 36,151-177 (1974).

6. Amiet, R., "Noise Produced by Turbulent Flow into a Propeller or Helicoper Rotor," AIAA J., 15,307-308 (1977).

7. Blake, W. B., MECHANICS OF FLOW-INDUCED SOUND AND VIBRATION, Vol. II Complex Flow-Structure Interactions, Academic Press, Inc. (1986).

8. Martinez, R., and K. Weissman, "Spatial-Domain Analysis of the Thrust on a Propeller Cutting Through Isotropic Turbulence," CAA Rept. U-1894-358.47 (1990).

9. Hinze, J. O., TURBULENCE, AN INTRODUCTION TO ITS MECHANICS AND THEORY, McGraw-Hill, New York (1959).

10. Sears, W. R., "Some Aspects of Non-Stationary Air Foil Theory and Its Practical Application," J. Aeron. Sci., Vol. 8 (1941).